A&A 388, 587–608 (2002)
DOI: 10.1051/0004-6361:20020503

Astronomy & Astrophysics

Wind variability of B supergiants

IV. A survey of *IUE* time-series data of 11 B0 to B3 stars

R. K. Prinja[1], D. Massa[2], and A. W. Fullerton[3,4]

[1] Department of Physics & Astronomy, University College London, Gower Street, London WC1E 6BT, UK
[2] Raytheon ITSS, NASA/GSFC, Code 681, Greenbelt, MD 20771, USA
e-mail: massa@taotaomona.gsfc.nasa.gov
[3] Department of Physics and Astronomy, University of Victoria, PO Box 3055, Victoria, BC V8W 3P6, Canada
e-mail: awf@pha.jhu.edu
[4] Center for Astrophysical Sciences, Dept. of Physics and Astronomy, Johns Hopkins University, 3400 N. Charles St, Baltimore, MD 21218-2686, USA

Received 11 January 2002 / Accepted 28 March 2002

Abstract. We present the most suitable data sets available in the *International Ultraviolet Explorer* (*IUE*) archive for the study of time-dependent stellar winds in early B supergiants. The UV line profile variability in 11 B0 to B3 stars is analysed, compared and discussed, based on 16 separate data sets comprising over 600 homogeneously reduced high-resolution spectrograms. The targets include "normal" stars with moderate rotation rates and examples of rapid rotators. A gallery of grey-scale images (dynamic spectra) is presented, which demonstrates the richness and range of wind variability and highlights different structures in the winds of these stars. This work emphasises the suitability of B supergiants for wind studies, under-pinned by the fact that they exhibit unsaturated wind lines for a wide range of ionization.
The wind activity of B supergiants is substantial and has highly varied characteristics. The variability evident in individual stars is classified and described in terms of discrete absorption components, spontaneous absorption, bowed structures, recurrence, and ionization variability and stratification. Similar structures can occur in stars of different fundamental parameters, but also different structures may occur in the same star at a given epoch. We discuss the physical phenomena that may be associated with the spectral signatures. The diversity of wind patterns evident likely reflects the role of stellar rotation and viewing angle in determining the observational characteristics of azimuthally extended structure rooted at the stellar surface.
In addition, SEI line-synthesis modelling of the UV wind lines is used to provide further information about the state of the winds in our program stars. Typically the range, implied by the line profile variability, in the product of mass-loss rate and ion fraction ($\dot{M}\, q_i$) is a factor of ∼1.5, when integrated between 0.2 and 0.9 v_∞; it can however be several times larger over localised velocity regions. At a given effective temperature the mean relative ion ratios can differ by a factor of 5. The general excess in predicted (forward-scattered) emission in the low velocity regime is discussed in terms of structured outflows. Mean ion fractions are estimated over the B0 to B1 spectral classes, and trends in the ionic ratios as a function of wind velocity are described. The low values obtained for the ion fractions of UV resonance lines may reflect the role of clumping in the wind.

Key words. stars: early-type – stars: mass-loss – ultraviolet: stars

1. Introduction

The radiation-pressure-driven winds of O and early-B type stars are variable on characteristic time-scales of hours and days, as a result of perturbations in the outflow due to small- and large-scale structure, respectively. Observable diagnostics of the former include extended black absorption troughs in saturated UV P Cygni profiles (Lucy 1983), X-ray emission (Lucy & White 1980; Feldmeier et al. 1997; Kahn et al. 2001; Cassinelli et al. 2001), and non-thermal radio emission (Bieging et al. 1989; Scuderi et al. 1998). The small-scale wind structures responsible for these signatures are believed to result from a strong instability in the line-driven winds, which operates on linear scales smaller than the Sobolev length. This instability leads to multiply non-monotonic velocity fields in the wind and localised density enhancements which are bounded by pairs of forward and reverse shocks

Send offprint requests to: R. K. Prinja,
e-mail: rkp@star.ucl.ac.uk

(e.g. Owocki et al. 1988; Feldmeier 1995). Large-scale structure in hot star winds is primarily studied via systematic variability of UV resonance and optical emission lines. These changes diagnose organised, spatially extended perturbations in the wind, which may be induced by magnetic or pulsational processes arising at the stellar surface. We document in this paper the nature of *large-scale* wind structure in 11 early-type B supergiant stars, based on high-resolution *International Ultraviolet Explorer* (*IUE*) time-series spectroscopy.

One of the major discoveries made with *IUE* was the systematic nature of variability in the P Cygni-type line profiles of OB stars. The key developmental sequence was defined in a number of time-series UV investigations (e.g. Prinja et al. 1987; Prinja & Howarth 1988; Henrichs et al. 1988; Kaper 1993; Kaper et al. 1996; De Jong et al. 2001). A relatively broad, shallow absorption feature appears at $\leq$0.3 of the terminal velocity (v_∞), which then evolves blue-wards over several hours and perhaps even days, while narrowing in velocity width. The velocity at which these "discrete absorption components" (DACs) are first detected is roughly constant for a given star, but may vary from star-to-star.

Subsequent *IUE* studies established a connection between stellar projected rotation velocity ($v_\mathrm{e}\sin(i)$) and the rate of recurrence and acceleration of DACs (Prinja 1988; Kaper et al. 1996). More recent *IUE* monitoring campaigns extending over a few weeks have shown that the stellar wind lines vary continuously, implying that OB star winds are structured over a range of spatial and temporal scales. They have also shown that variations in the profiles modulate on rather long time-scales (i.e. several days). Furthermore, the variability evident in ξ Per (O7.5 III(f); De Jong et al. 2001) and ζ Pup (O4 If; Howarth et al. 1995) appears to modulate on the stellar rotation rate. Rotation is plausibly also the key factor in the repetitive wind activity seen in HD 64760 (B0.5 Ib; Fullerton et al. 1997), HD 93843 (O5 III; Prinja et al. 1998) and HD 91969 (B0 Ia; Massa et al. 1998). Rotationally modulated wind fluctuations are also apparent in late B and early A supergiants (e.g. Kaufer et al. 1996), which have much larger radii and longer rotation periods.

The fundamental origin of wind variability on large spatial scales in hot stars remains uncertain. The causal link between inhomogeneities at the stellar surface and large-scale wind structure has not been directly established observationally or theoretically. A currently popular idea is that the large-scale variations discussed above (and some of those discussed in this paper) are spawned by photospheric irregularities which cause the wind from different longitudinal sectors on the surface to emerge with different densities and/or velocities. The surface structure may, for example, be due to the action of non-radial pulsations or the effects of ordered magnetic fields. Once different adjacent wind streams are initiated, they then meet to form co-rotation interaction regions (CIRs). The rotating CIRs inevitably evolve into spiral-shaped shock structures (Cranmer & Owocki 1996). In this model, variations in the wind absorption result from material flowing through a semi-permanent, co-rotating wind structure.

1.1. Winds of early B-type supergiants

The stellar winds of early B supergiants (BIs) are particularly suitable for a study of wind dynamics and the effects of large-scale wind structure since, (i) their UV wind lines are often well-developed but unsaturated, (ii) these diagnostic lines cover a wide range of ionization, close to the dominant stage of the wind (see Table 2), (iii) it is generally easier to follow the progression of large-scale structure in the UV lines of BIs compared to O-type stars, (iv) the winds have lower terminal velocities, so individual structures evolve more slowly and the important Si IV $\lambda\lambda$1400 resonance line doublets are mostly decoupled, (v) their strong UV photospheric lines are excellent effective temperature–luminosity diagnostics, and (vi) the strongest UV photospheric lines sample the wind/photosphere "interface", often displaying wind behaviour.

Motivated by these attractions, we describe in this paper the time-dependent wind characteristics of eleven B0 to B3 supergiants, based on 16 separate *IUE* high-resolution time-series data sets, involving the inspection of 638 spectrograms in total. This work extends our knowledge of the characteristics of variable UV resonance lines in line-driven winds to cooler and less luminous stars. The data are used to demonstrate the presence of a range of empirical wind properties and implied varied perturbations in the outflows. We report here on the incidence and repetition of DACs, evidence for rotational modulation, ionization-state changes, shock formation, and spontaneous wind enhancements. The diverse wind variability signatures in early BIs are compared and contrasted to those previously noted in luminous O-type stars. The later sections of this paper present SEI line-synthesis modelling, which is used to explore further the ionization mixture and structured nature of the winds.

2. The IUE time-series data sets

Our objective was to carry out a systematic survey of the temporal nature of wind activity in early B supergiants. We therefore restricted our selection to time-series of high-resolution ($\lambda/\Delta\lambda \sim 10^4$) *IUE* SWP ($\lambda\lambda$1150 to 1900 Å) data sets. A list of the program stars is given in Table 1. They include luminosity classes Ia and Ib for a spectral range B0 to B3, and have a wide range of projected rotation velocities. The corresponding 16 data sets analysed are also outlined in Table 1, and include 4 cases where short-term wind variability may be compared over two or more epochs separated by a few years. The majority of stars in our sample are "normal", slow to moderate rotators, that are representative of their spectral subclass. Two main exceptions are HD 64760 and HD 157246 (γ Ara) which were selected to examine the effects of rapid rotation on wind structure.

Table 1. Program stars.

HD	Sp. Type	$\mathrm{Log}(L_*/L_\odot)$	$T_{\rm eff}$ (kK)	$v_{\rm e}\sin(i)$ (km s^{-1})	$P_{\rm rot}$ (max) (days)	Date of IUE time series	Duration (days)	Sampling (hours)
37128	B0 Ia N$^-$	5.78	28.6	91	17.7	1980	0.7	1
91969	B0 Ia	5.78	28.6	83	14.4	1996	30	9
164402	B0 Ib N$^-$	5.38	28.6	77	13.3	1986/93/95	6/16/16	3–24/24/24
204172	B0 Ib N$^-$	5.38	28.6	87	11.6	1990/93	2/16	3/24
64760	B0.5 Ib	5.10	23.1	216	5.2	1993/95	6/15	3/3
167756	B0.5 Ib	5.50	23.1	79	14.1	1986	5.5	12
150168	B1 Iab-Ib	5.38	20.3	121	13.3	1993	6	3
47240	B1 Ib	4.90	20.3	103	11.3	1993	16	24
157246	B1 Ib	4.90	20.3	245	4.8	1993/95	6/16	3/24
96248	BC1 Ia	5.12	19.4	83	24.3	1996	30	9
53138	B3 Ia	5.24	16.3	58	45.8	1987	13	12–36

$T_{\rm eff}$ and $\mathrm{Log}(L_*/L_\odot)$ from Humphreys & McElroy (1984); $v_{\rm e}\sin(i)$ from Howarth et al. (1997). Spectral types from Walborn (1972, 1976), Garrison et al. (1977), Hiltner et al. (1969), and Morgan et al. (1955). N$^-$ refers to stars whose spectra are nitrogen deficient. $P_{\rm rot}$(max) is the estimated maximum rotation period of the star.

The data were either extracted from the archives maintained at the Goddard Space Flight Center (USA) and the Rutherford Appleton Laboratory (UK), or they were originally part of our observing campaigns. All the spectra were extracted in a uniform manner from the two-dimensional, photometrically linearised images (PI) using the UK Starlink package *IUEDR* (Giddings et al. 1995). One of the advantages of the *IUEDR* extractions is the spectra are highly reliable at the shortest wavelengths, thus providing high data quality for the important lines at Si III λ1206 and N V $\lambda\lambda$1240. The wavelength scale calibration was improved by centering the spectra on selected interstellar lines (in an échelle order-dependent correction). The individual spectra were binned onto a wavelength grid with a regular sampling of 0.1 Å. Typically the signal-to-noise in the continuum is ∼20. Individual wind-formed line profiles were normalised to a local continuum by fitting a straight line through several adjacent "line-free" windows.

The mean *IUE* SWP spectrum for each program star is shown in Fig. 1. The principal diagnostic wind and photospheric lines available in these spectra are listed in Table 2 (Massa 1989). The data sets for the following stars have been previously reported in the literature: HD 64760 (Massa et al. 1995b; Prinja et al. 1995; Fullerton et al. 1997; Howarth et al. 1998), HD 157246 (Prinja et al. 1997), and HD 91969 (Massa et al. 1998). These data are presented in this paper to place them into wider comparative context.

3. Time-dependent stellar wind phenomena

The characteristics of variable UV lines in our program stars are presented in this section. Fluctuations are present in the stellar wind lines of *every* B supergiant in our sample, and in every time-series data set examined here. The variations are primarily described by a gallery of grey-scale image representations (dynamic spectra) of the time-series data (Figs. 2 to 17). This image format is an effective method for identifying systematic patterns in variable line profiles, and for comparing the evolution of these features between different spectral lines. In cases where the Doppler shifted absorption profiles are unsaturated (i.e. the majority in our sample), quotient spectra are displayed after being normalised by the mean profile for the time-series. For saturated or "black" absorption troughs in the C IV lines of HDs 37128, 91969, 157246 and 96248, we display residuals, subtracted from the mean profile. In all cases darker shades in the images indicate regions of enhanced absorption (reduced flux) with respect to the mean profile.

3.1. List of observed stellar wind phenomena

Several empirical phenomena can be identified from the images in Figs. 2 to 17. They are defined below, prior to discussion of their occurrence in individual stars:

Discrete absorption components (DACs) – these are the features most commonly associated with variable UV resonance line profiles in luminous OB stars. They usually appear as localised (in velocity) absorption enhancements that migrate from (at least) intermediate velocities to the blue-ward profile edge, with a corresponding decrease in velocity width. Typically the accelerations of the DACs are $\leq$50% of values for the underlying wind, as determined from canonical "$\beta \sim 1$" velocity laws.

Bowed structures – these are optical depth changes that appear suddenly over a wide velocity range, and which develop simultaneously towards lower and higher blue-shifted velocities (see e.g. Fullerton et al. 1997).

Other features – we use this term to identify either less organised "bursts" of absorption that usually last a short time only (hours), or more substantial absorptions that appear suddenly over a large velocity range. These features do not show any clear evolution in their velocity or width as a function of time.

Near-zero velocity changes – cases where line profile variability can be traced to less than 0.05 of the terminal

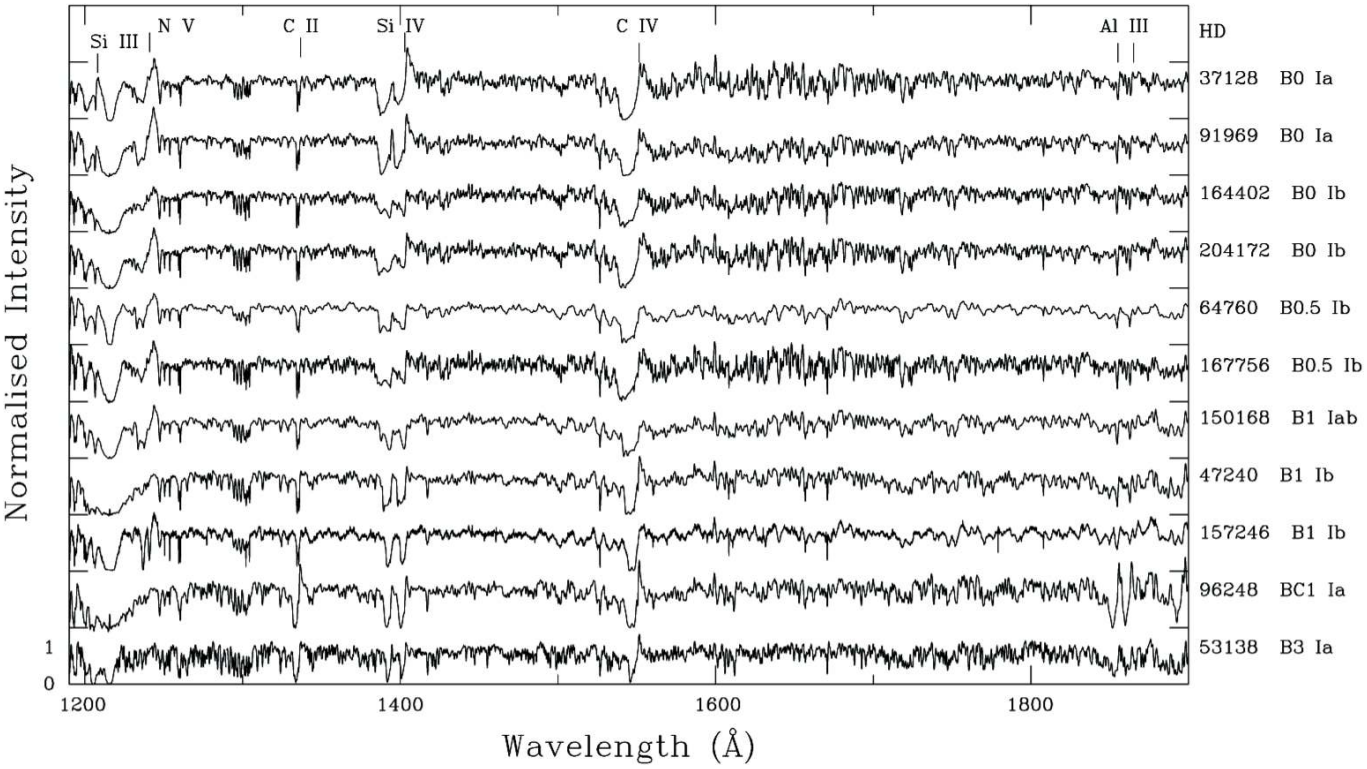

Fig. 1. Mean normalised spectra for the *IUE* time-series of the 11 program stars. The important wind spectral lines are identified (see also Table 2). (An intensity shift of 1.5 has been used in this display between successive spectra.)

Table 2. Key *IUE* line diagnostics for early-B supergiants winds.

Ion	λ_0 (Å)	I.P. (ev)	E.P. (eV)	region
C II	1334.53, 1335.71	24.4	0.00, 0.01	wind
C IV	1540.20, 1550.77	64.5	0.0, 0.0	wind
N V	1238.82, 1242.80	97.9	0.0, 0.0	wind
Al III	1854.72, 1862.79	28.5	0.0, 0.0	wind
Si III	1206.50	33.5	0.0	wind
Si III	1296.73	33.5	6.55	wind/photosphere
Si III	1312.24	33.5	10.28	photosphere
Si III	1417.24	33.5	10.28	photosphere
Si IV	1393.76, 1402.77	45.1	0.0, 0.0	wind

velocity. These fluctuations are due to deep-seated disturbances close to the stellar surface.

Recurrence – This is simply a descriptive term relating to a specific (extended) data set, to draw attention to repetitive structures. The repetition is normally due to the occurrence of DACs or bowed structures.

Ionization variation – implies that the ionization state of a specific wind feature changes with time. It may for example become more enhanced in absorption in some lines, while exhibiting an increased flux in other spectral lines.

Ionization stratification – cases where one of the phenomena identified above are seen at different velocities in different ions. This is usually an optical depth effect between low and high ionization lines.

Results on the occurrence of these variable wind phenomena in our program stars are summarised in Table 3. The winds of early BIs exhibit diverse patterns of stellar wind variability. Similar phenomena can occur in stars that vary in fundamental parameters, and different wind structures can co-exist in the wind of a given star at a particular epoch. Some notes on the temporal wind behaviour in the individual stars are presented in the remainder of this section.

3.2. Notes on individual stars

HD 37128 (ϵ Ori, B0 Ia N$^-$; Fig. 2). A well-studied, moderately nitrogen weak star (Walborn 1976), part of the Ori OB1 association. ϵ Ori has been cited as a single-lined spectroscopic binary (e.g. Frost 1909; Morrell & Levato 1991), however its binarity remains uncertain and, for example, Jarad et al. (1989) found it to be a radial velocity

Table 3. Observed stellar wind phenomena.

HD	DAC	Bowed structure	Other feature	near-zero var.	ion strat.	ion var.	recurrence
37128	√	–	–	–	–	–	–
91969	√	–	√	√	√	√	√
164402	√	–	√	?	–	–	–
204172	?	–	√	?	–	–	–
64760	√	√	√	√	√	√	√
167756	√	–	√	√	√	–	–
150168	√	√	√	√	√	√	√
47240	√	–	√	√	√	–	–
157246	√	–	√	–	√	√	–
96248	√	–	√	–	√	–	–
53138	√	–	√	–	–	–	–

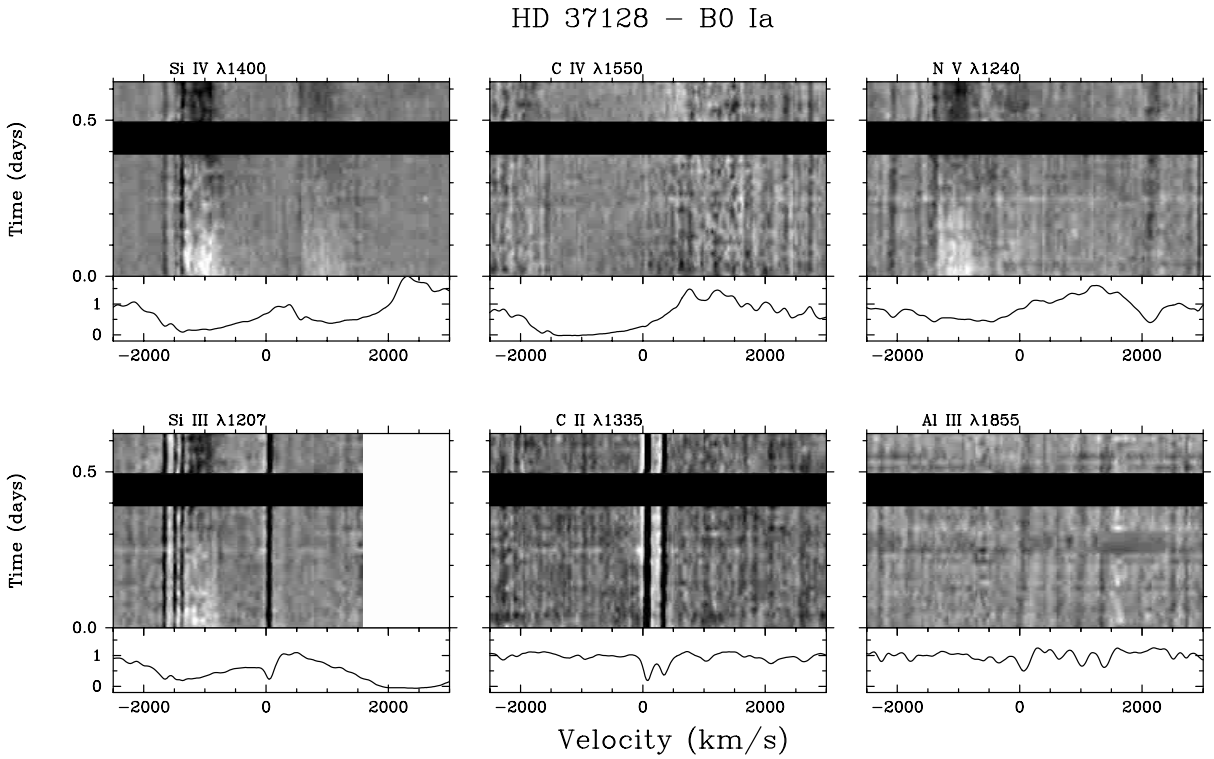

Fig. 2. Grey-scale representation of variability in HD 37128.

constant. Variability in the hydrogen lines has been reported by Gry et al. (1984) and Ebbets (1982). Previous suggestions that it is a variable thermal radio source are discounted by Blomme et al. (2002).

UV variability in the short intensive *IUE* time-series is shown in Fig. 2. We note the progression of a DAC feature between ∼−900 to −1200 km s^{-1} over ∼14 hours. High velocity narrow absorption components are also present towards the short-ward edge. Strong photospheric lines (e.g. C III 1247 and Al III 1855) reveal radial velocity shifts of ∼20 km s^{-1}.

HD 91969 (B0 Ia; Fig. 3). A member of the Car OB1 association (e.g. Humphreys 1978). It is one of the brightest members of the NGC 3293 open cluster in the Carina region (e.g. Feinstein & Marracu 1980). The *IUE* time-series data studied here were secured during our "MEGA II" campaign in 1996, and some of our findings have been summarised by Massa et al. (1998). This star is an excellent example of the variety of diagnostic UV lines available in early BIs. Massa et al. (1998) reported a 7.8-days period for the repetition of DAC features propagating blue-ward toward the profile edge. These features are seen at very low velocities in Al III, and their progression "connects" with corresponding events seen at higher velocities in Si III, Si IV and N V. There is however evidence for ion stratification between activity in Al III and Si IV. The temporal coherency is strongest in the low ion species which form in the deeper regions of the wind. The periodic line profile changes are seen down to very low velocities (less than 0.05 v_∞), together with variations in photospheric lines

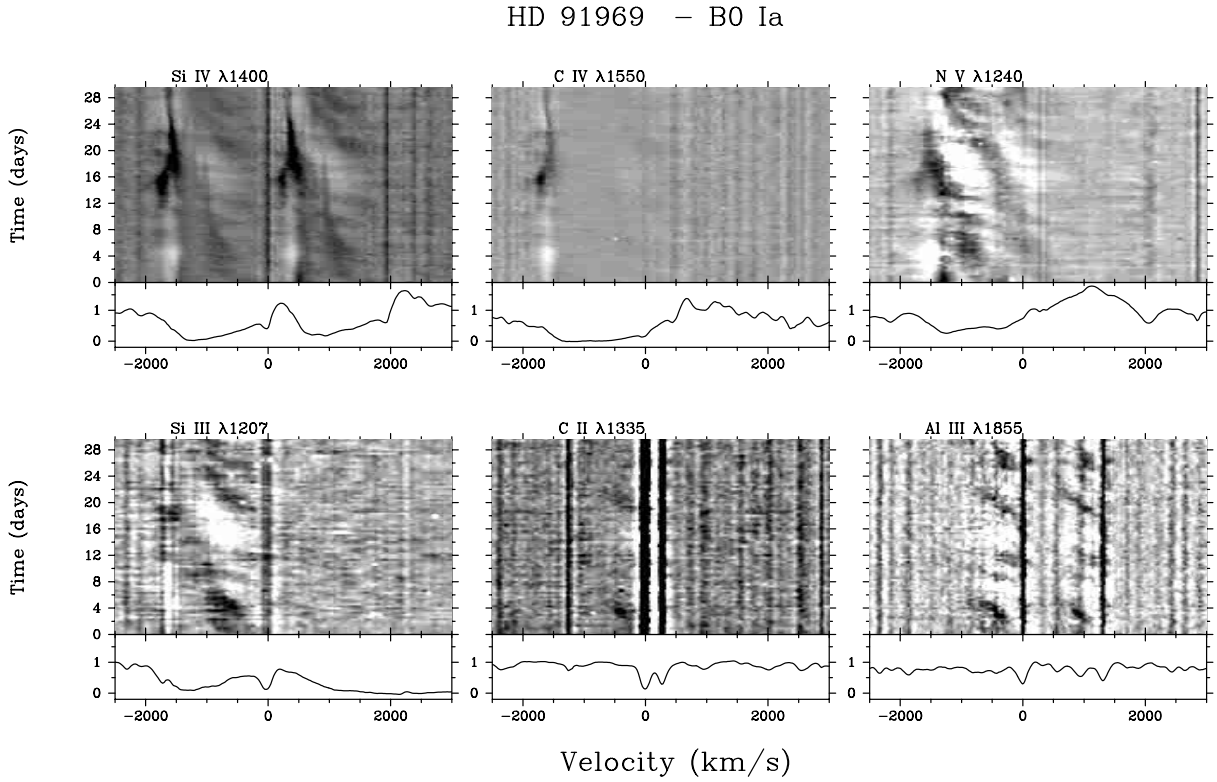

Fig. 3. Grey-scale representation of variability in HD 91969.

due to Si III, Fe III, and Fe IV. The latter may be tracers of localised surface inhomogeneities responsible for wind activity.

HD 164402 (B0 Ib N$^-$; Figs. 4 to 6). A member of the Sgr OB1 association (Humphreys 1978), this star has one of the lowest projected rotation velocities in our sample. It is moderately nitrogen deficient, with no indication of binary companionship (e.g. Levato et al. 1988). HD 164402 provides an opportunity to study systematic wind activity over three separate epochs. The 1986 data set (Fig. 4) has a poorer temporal sampling, but reveals a distinctive DAC progressing from $\sim$−1200 km s^{-1} to $\sim$−1600 km s^{-1} over 6 days. This feature is accompanied by more sporadic events, which are well spread in velocity, but unresolved temporally (e.g. at $T \sim 3.5$, 4,2 and 5 days, where T is time relative to the first observation in the series). The 1993 time-series (Fig. 5) spans almost 16 days and reveals a remarkably slowly migrating DAC, with a mean acceleration of $\sim 3 \times 10^{-4}$ km s^{-2}. Other features with different characteristics and more rapid evolution are also noted at $T \sim 6$ and 12 days. Drastic variations are present in the 1995 data set (Fig. 6) around $T \sim 14$ days. The highest velocity absorption (at $\sim$−1750 km s^{-1}) suddenly decreases and is accompanied by lower velocity DAC features at $\sim$−1300 km s^{-1} and −1000 km s^{-1}. The sudden reversal in optical depth across the lines may represent the signature of a large scale shock.

HD 204172 (69 Cyg; B0 Ib N$^-$; Figs. 7, 8). A moderately nitrogen weak star (Walborn 1976), belonging to the Cyg OB2 association. Lennon et al. (1992) highlight several discrepancies between the B0 Ib spectral type assignment and the appearance of the optical spectral line profiles, including H lines being too narrow and Si IV too strong. They suggest a revision to B0.2 Ia. The UV resonance lines of 69 Cyg are generally stronger than those of HD 164402, thus favouring a slightly more luminous spectral type. The densely sampled 1990 time series (Fig. 7) reveals a gradual increase in profile absorption strength over $\sim$2.2. days. The fluctuations extend over a broad velocity range that cover almost the entire Si IV absorption trough. Corresponding changes are seen at much lower velocity (extending close to zero velocity) in C II λ1335 and Al III λ1855. The velocity differences between low and high ions are principally an optical depth effect. There are also traces of DAC features at $\sim$−1700 km s^{-1} (e.g. $T \sim 0$ to 0.5 days) in Si IV, C IV and N V. Some changes are apparent in the strong C III λ1247 "photospheric" line. The 1993 data set (Fig. 8) is more extended and covers almost 16 days. Two enhanced absorptions are present over a substantial velocity range. These may be similar events to the phenomena seen with greater time resolution in 1990 (Fig. 7). There is a tentative indication that the feature recurs over $\sim$12 days, which is close to the estimated maximum rotation period of the star (Table 1). Some variations are also noted in the deep-seated C III λ1247 and Si III λ1300 triplets.

HD 64760 (B0.5 Ib; Figs. 9, 10). This is one of two rapid rotators in our sample. The data sets for the two epochs shown here were discussed in detail by Massa et al. (1995b) and Fullerton et al. (1997). HD 64760 exhibits a variety of

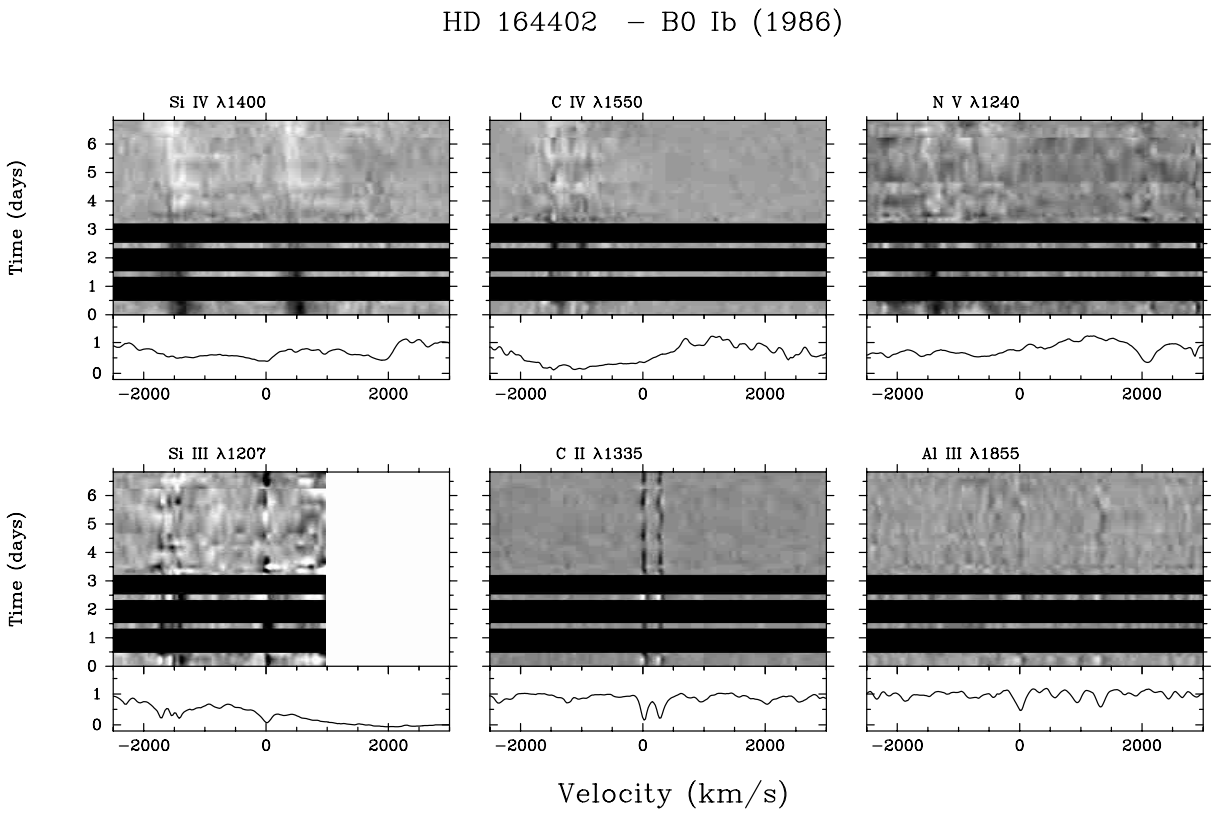

Fig. 4. Grey-scale representation of variability in HD 164402 (1986).

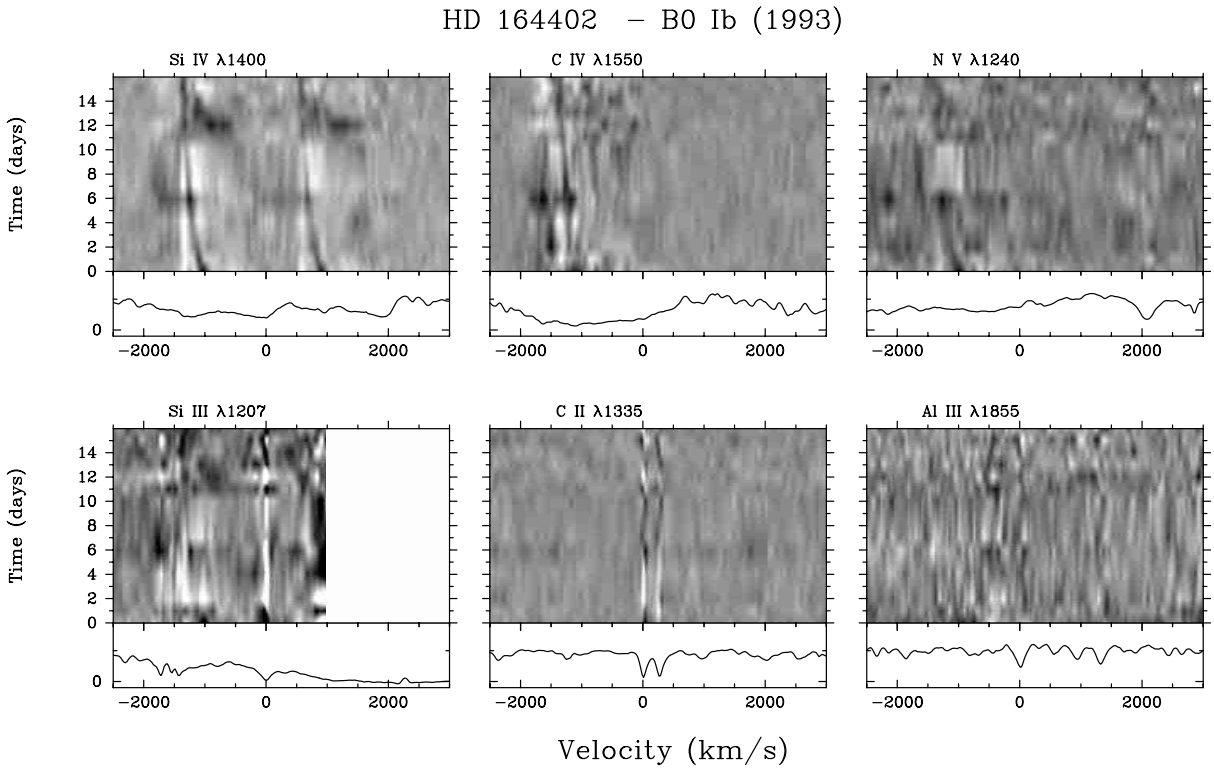

Fig. 5. Grey-scale representation of variability in HD 164402 (1993).

spectral features that indicate co-existing wind structure. In fact, every category of stellar wind phenomena listed in Table 3 is present in this star! The "MEGA I" campaign during 1995 (Fig. 10) in particular reveals a striking 1.2-day modulation, where individual features cover a large velocity range, and have a bow-shaped morphology

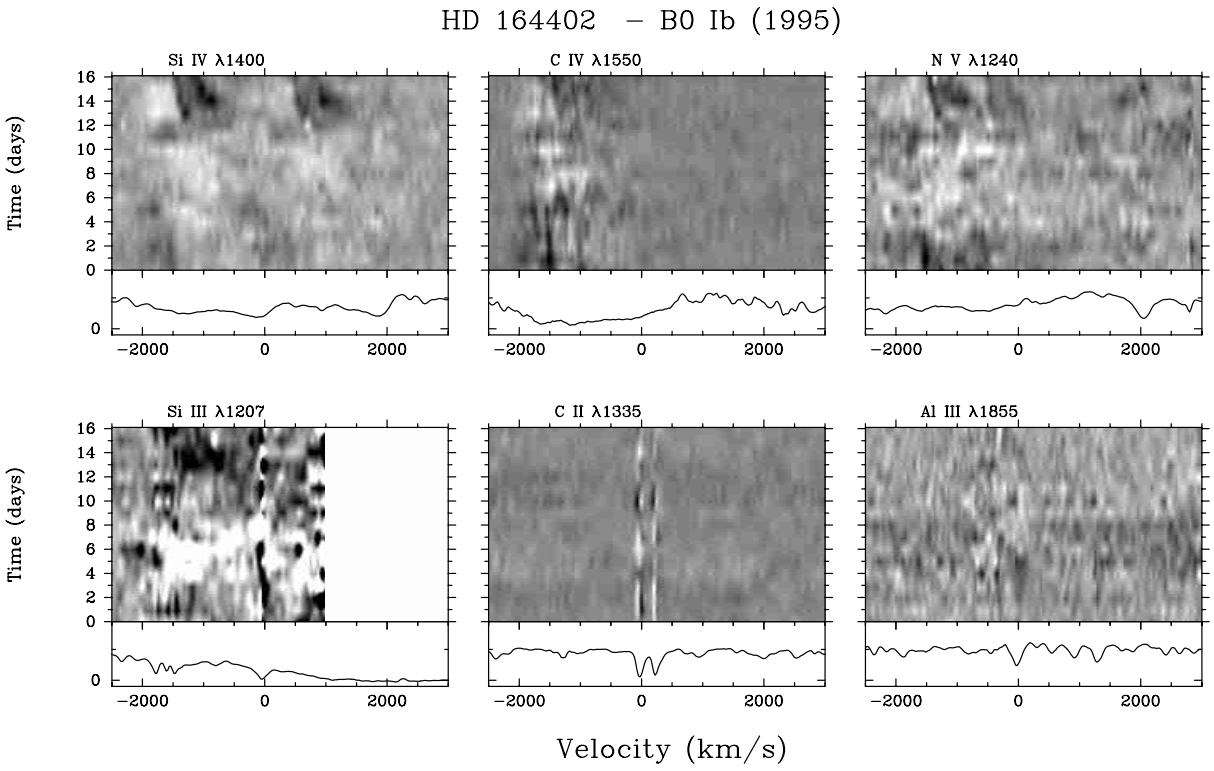

Fig. 6. Grey-scale representation of variability in HD 164402 (1995).

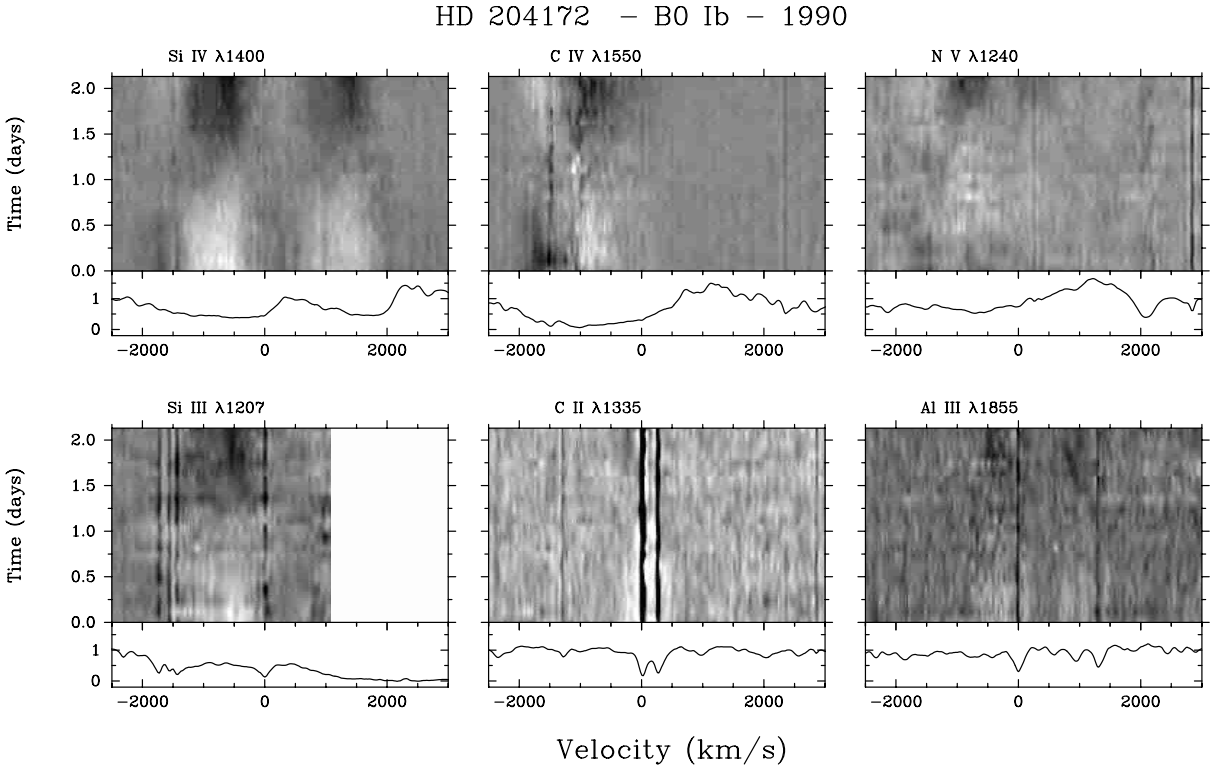

Fig. 7. Grey-scale representation of variability in HD 204172 (1990).

such that they extend blue-wards and red-wards at the same time. Ionization variability is indicated by the fact that the N V data appear to have nearly twice the modulation frequency of Si III (Fullerton et al. 1997). Slower migrating, high velocity DACs are also present, which persist over several days. The recurrence time-scale for the DACs is not constrained. An exceptionally strong absorption event is present in high-ion species in the (shorter)

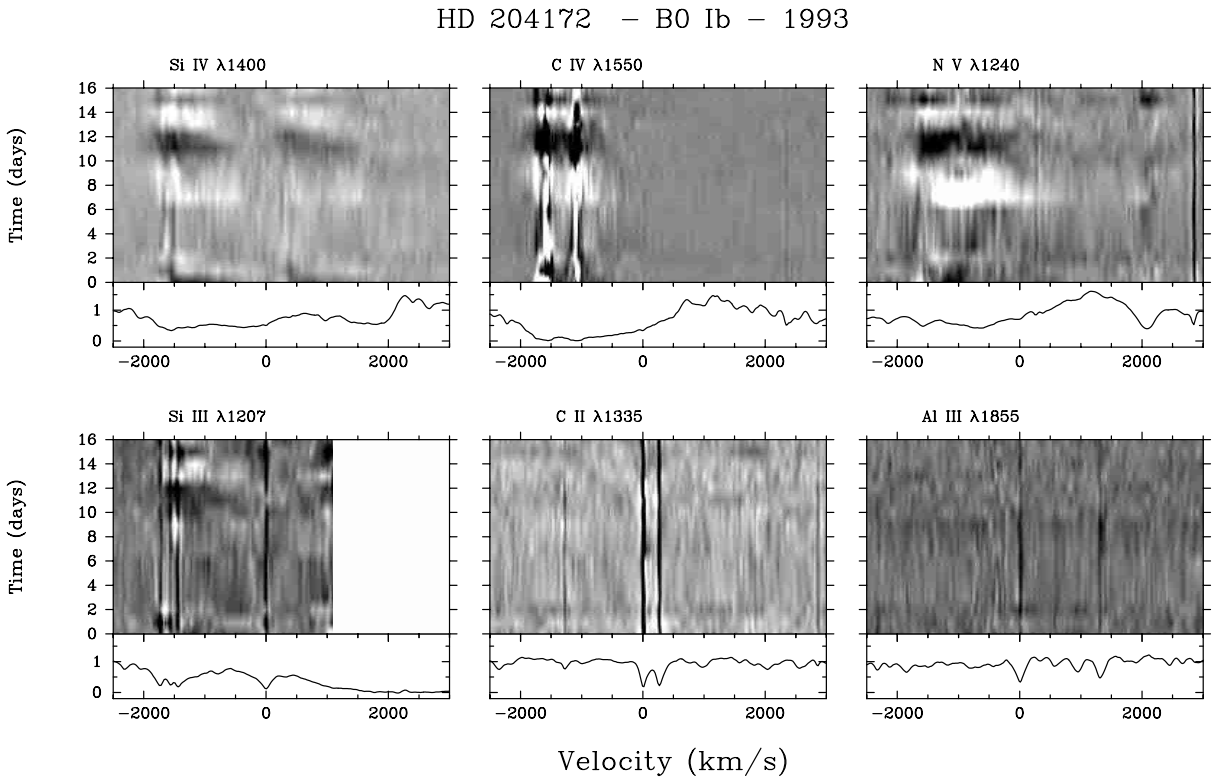

Fig. 8. Grey-scale representation of variability in HD 204172 (1993).

time series data for 1993 (Fig. 9, around $T \sim 2$ days). It is accompanied by variations essentially down to zero velocity in e.g. C II $\lambda\lambda$1335 and Al III λ1855, plus disturbances in the "photospheric" Si III λ1300 triplets. The onset of these substantial changes is also marked by changes in the relative ionization mixture, such that the overall ionization of the wind increases during this event (Massa et al. 1995b). It is possible that this strong event, and the overall enhancement seen at $T \sim 4$ days (Fig. 9), are similar to the bowed structures apparent in the more extensive MEGA I data set (Fig. 10).

HD 167756 (B0.5 Ib; Fig. 11). A distant halo star, located about 4 kpc away at a Galactic altitude of −0.85 Kpc (e.g. Savage & Massa 1985). Ionization shifts are apparent in the wind-formed lines, with the high velocity ($\sim$−1500 km s^{-1}) DAC seen in Si IV ($T \sim 0$ to 3 days) only being apparent at less than −500 km s^{-1} in Al III. The absorption enhancement seen in Si IV, N V, and C IV towards the end of the observing run ($T \geq 4$ days) may also be accompanied by variations close to zero velocity in Si III λ1207 and Al III λ1855.

HD 150168 (B1 Iab-Ib; Fig. 12). A member of the Ara OB1 association (Humphreys 1978). The UV time-series reveals a radial velocity motion in strong UV photospheric lines (e.g. C III λ1247) due to binary motion. Several interesting wind effects are apparent in this star. Near the start of the time-series there is a maximum in absorption in N V which corresponds to a minimum in Si IV (i.e. ionization variability). Close to $T \sim 4$ days a bowed structure is present, with the absorption minimum in N V lagging the Si IV minimum (i.e. ion stratification). A much weaker bowed feature may be present at $T \sim 2$ days. Multiple high velocity DACs ($\geq$−1500 km s^{-1}) are seen in Si IV, C IV and N V.

HD 47240 (B1 Ib; Fig. 13). A member of the Mon OB2 association. Binary radial velocity motion is seen in strong UV photospheric lines (e.g. C III λ1247). The double DAC feature seen at the start of the time-series at $\sim$−700 km s^{-1} in Si IV is present at a lower velocity ($\leq$−500 km s^{-1}) in C II and Al III. This enhancement is seen at almost zero velocity in C IV, however there is very little line flux in Si III λ1207. The variations in Si IV between $\sim$−500 and −1000 km s^{-1} may be repetitive over a 3 to 5 day time scale.

HD 157246 (γ Ara, B1 Ib; Figs. 14, 15). This star has the highest projected rotation velocity in our sample of stars (Table 1). The 1993 UV time-series was discussed by Prinja et al. (1997; see Fig. 14). The data reveal a complex pattern of co-existing discrete features at low velocities (red-ward of −750 km s^{-1}) and high velocities (blue-ward of −1500 km s^{-1}). These regions are "divided" by the appearance of a very sharp (in velocity width) DAC-like feature. The location of this narrow feature is shifted by $\sim$400 km s^{-1} between Si IV and Al III (or C III). The two-component wind properties, and overall profile morphologies, suggest evidence for an equatorially compressed wind, with structure in the polar components (Prinja et al. 1997). The narrow DAC-like feature is not seen in the 1995 *IUE* time-series (Fig. 15), and the high speed wind between −1000 and −1500 km s^{-1} is also no longer present.

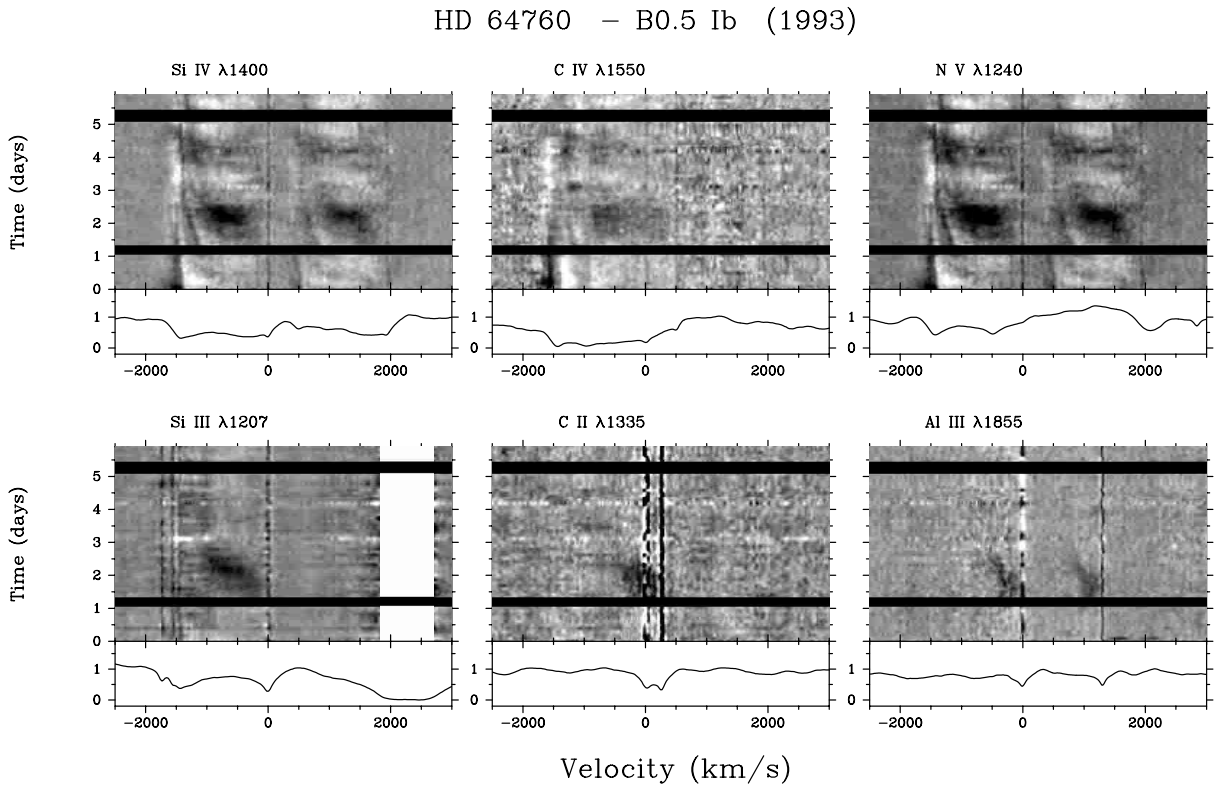

Fig. 9. Grey-scale representation of variability in HD 64760 (1993).

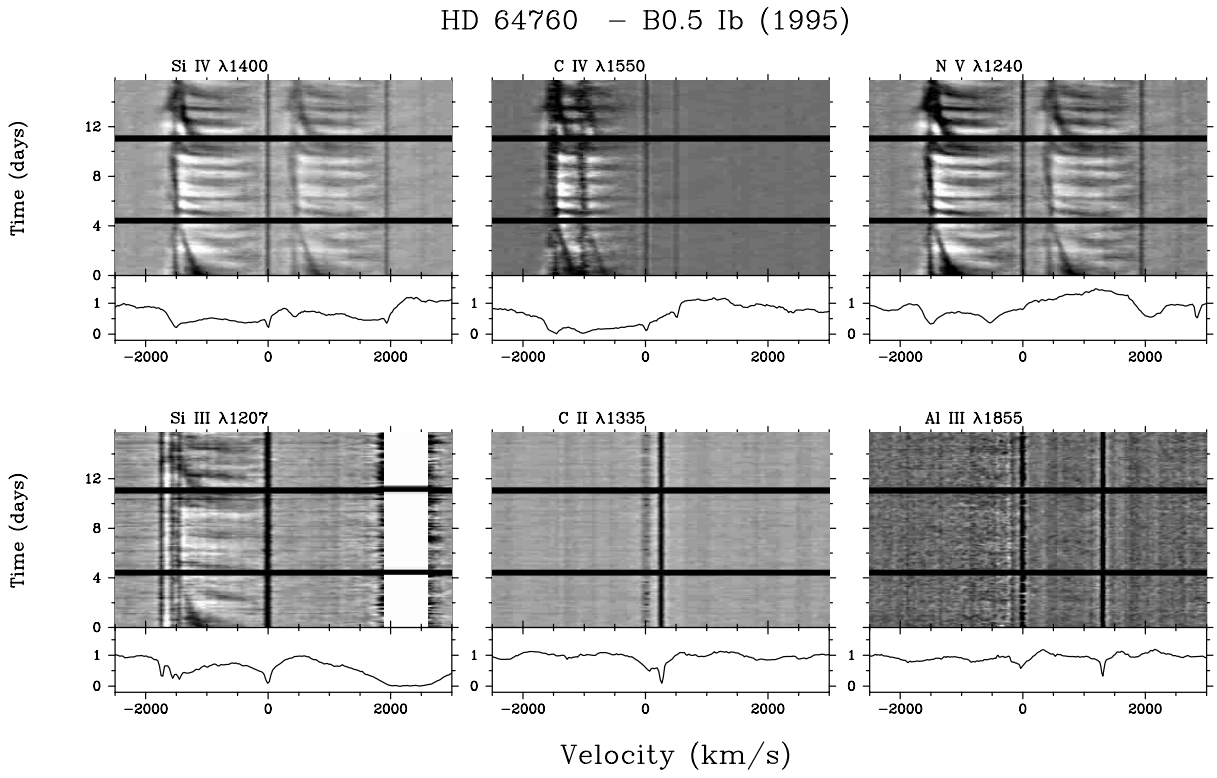

Fig. 10. Grey-scale representation of variability in HD 64760 (1995).

The line profiles in the 1995 data are more representative of the normal state of γ Ara (e.g. when compared to isolated archival spectra taken at earlier epochs). Some ionization state variability is observed between Si IV and N V (see e.g. the fluctuations between $T \sim 2$ to 8 days in Fig. 15). In both data sets variations are present down to near-zero velocities in the low ions.

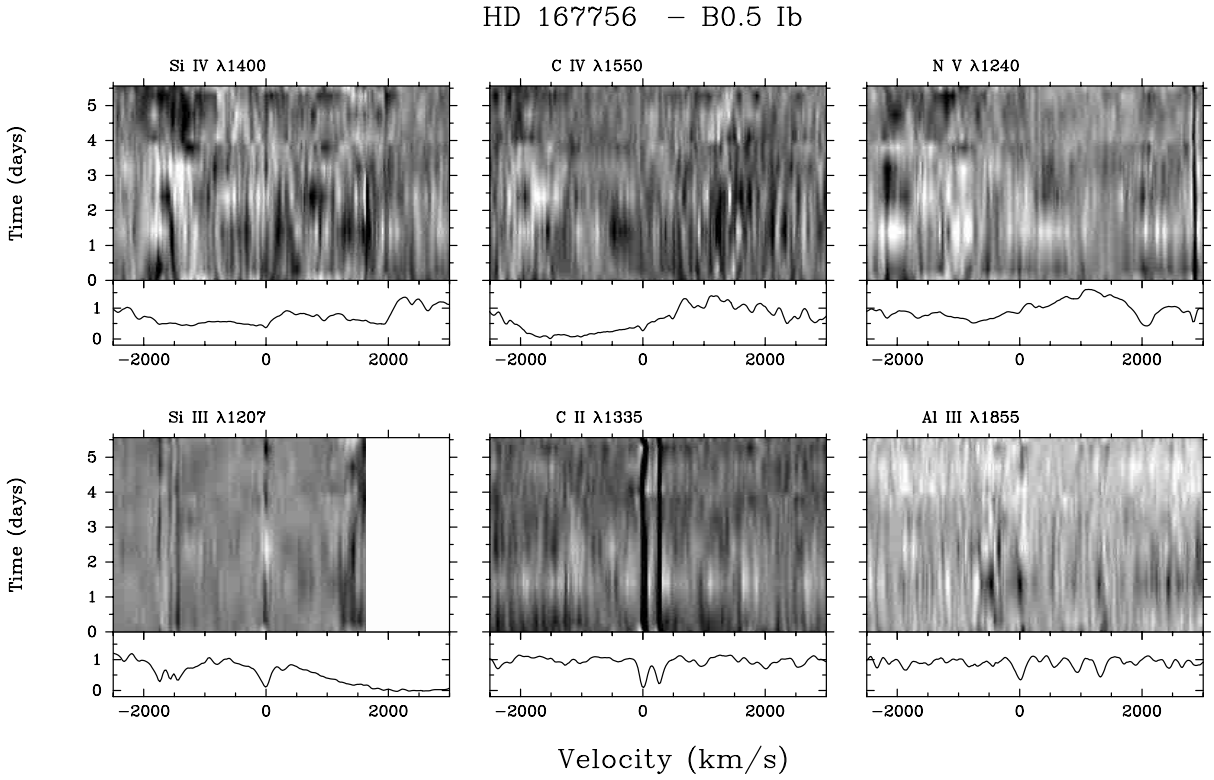

Fig. 11. Grey-scale representation of variability in HD 167756.

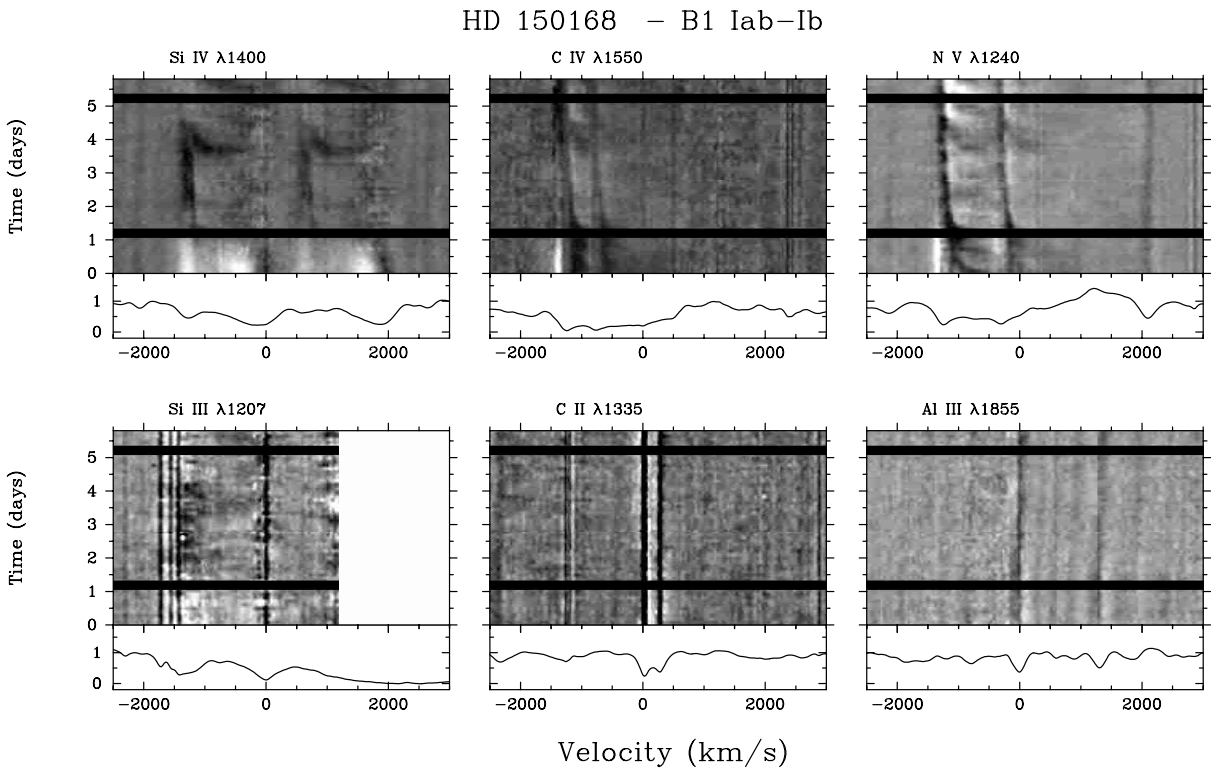

Fig. 12. Grey-scale representation of variability in HD 150168.

HD 96248 (BC1 Ia; Fig. 16). Carbon enhancement has been reported in this star by Dufton (1972) and Walborn (1976). HD 96248 is a radial velocity constant (e.g. Levato et al. 1988). The ∼30 day time-series shown in Fig. 16 is from the "MEGA II" Campaign of 1996. The Si IV and C IV profiles are nearly saturated, and the line

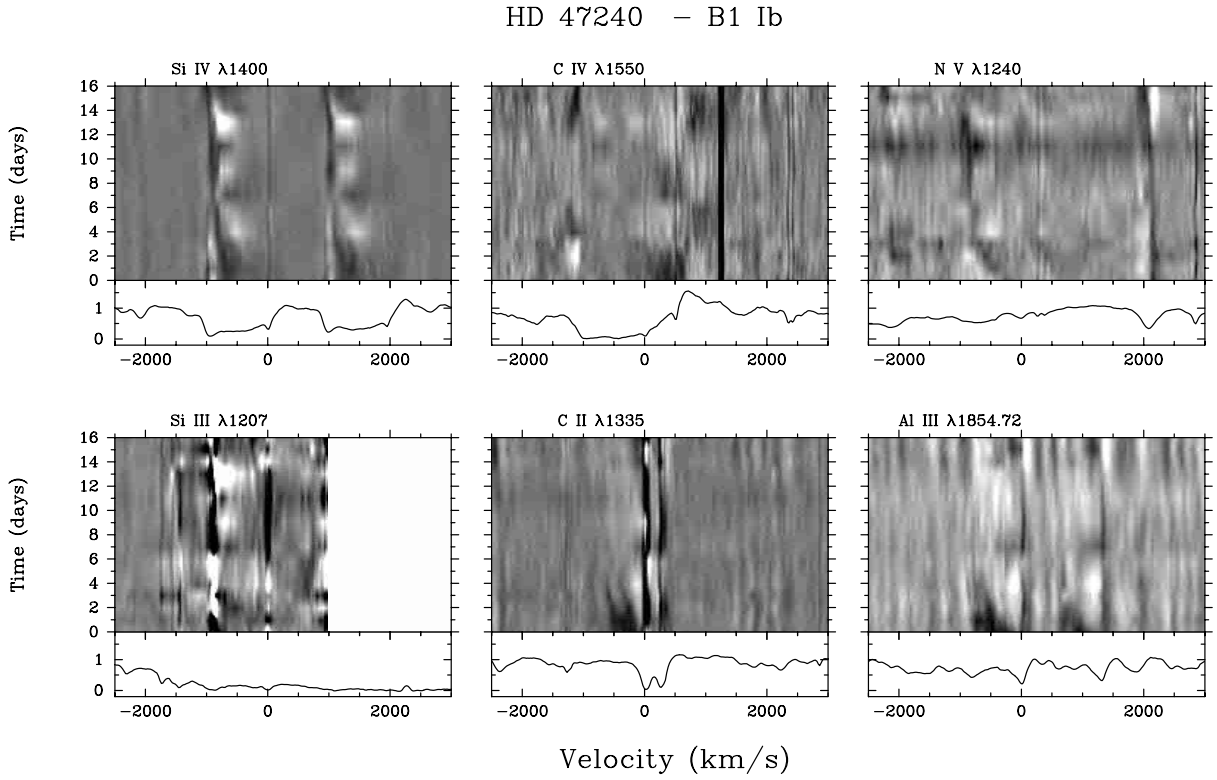

Fig. 13. Grey-scale representation of variability in HD 47240.

profile variability is confined to the blue edges (i.e. ≥ -750 to -1000 km s^{-1}). A gradual increase in absorption in the blue edge occurs from the start of the time-series to almost the end of the run, only weakening slightly after $T \sim 24$ days. These variations are mimicked in the low ions (Al III and C II), but at slightly lower velocities. Additional variations due to DACs are also seen between ~ -200 and -600 km s^{-1} in Al III, but they do not evolve into the structure seen at high velocities. The blue edge in C II λ1335 is not as shallow or extended as in the other lines.

HD 53138 (o^{2}CMa, B3 Ia; Fig. 17). A member of the Coll 121 association. HD 53138 exhibited very complex and highly variable characteristics in the Hα profile survey of Ebbets (1982), with variable absorption and emission components. Low velocity (red-ward of -500 km s^{-1}) UV variability is present in the $\sim$13 day time series shown in Fig. 17. A DAC feature is present between $T \sim 0$ to 4 days, which is essentially confined to high velocities. Various sporadic changes are apparent later in the run. Some degree of ion stratification is present, such that C II variations during the first 4 days appear at lower velocities than in Al III.

4. Comparisons

It is clear from Figs. 2 to 17 (and Table 2) that the stellar wind activity in early B supergiants, as revealed by the UV resonance lines, is substantial and has highly varied characteristics.

It is interesting to compare the BI wind activity presented here with that of 10 O-type stars described by Kaper et al. (1996), also based on high-resolution *IUE* spectroscopy. The O stars generally do not exhibit such a variety of temporal phenomena, and in particular show limited evidence for ionization related effects. (The comparisons are restricted, however, since Si IV is often the only reliable indicator of wind activity in O-type stars, as N V and C IV are saturated and the sub-ordinate N IV 1718 is only weakly present.) The fundamental characteristic patterns of variability in the O star data are in the form of blue-ward migrating DACs, though their properties may differ a lot between e.g. acceleration rates, multiplicity, and line-of-sight velocity dispersions. The coherence of systematic structure is generally greater in the UV lines of BIs compared to those of O stars. In terms of clearly defined – obviously modulated – wind structure, the B supergiant examples of HD 64760 and HD 91969 described above, are best matched by the O7.5 III stars ξ Per (HD 24912) and 68 Cygni (HD 203064).

In order to quantify the extent of variability as a function of velocity, we computed the temporal variance spectrum (TVS, see Fullerton et al. 1996) for the Si IV line profile for all our program stars:

$$(TVS)_i = \sigma_0^2 \frac{1}{N-1} \sum_{j=1}^{N} \left(\frac{S_{ij} - \bar{S}_i}{\sigma_{jc}\sqrt{\bar{S}_{ij}}} \right)^2 , \quad (1)$$

where S_{ij} is the normalized intensity of the ith pixel in the jth spectrum, $\bar{S}_i$ is the weighted mean of the normalized intensity, σ_{jc} is the inverse of S/N of

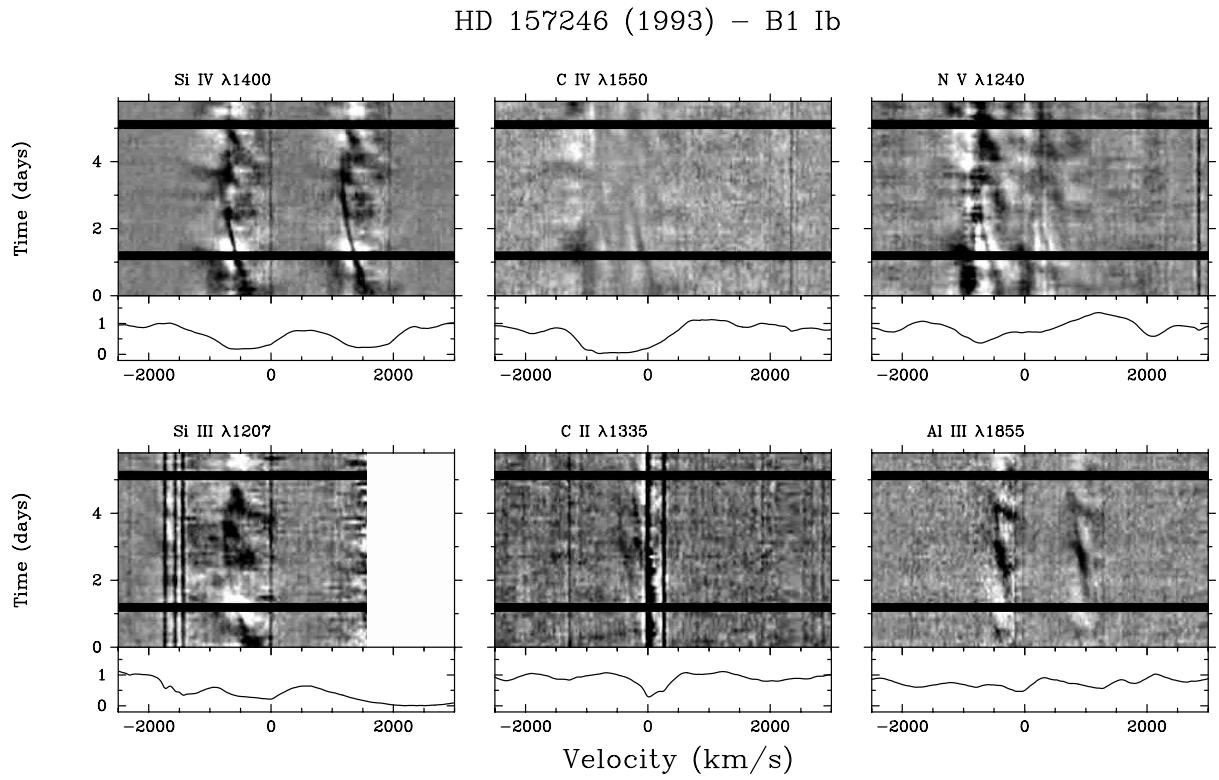

Fig. 14. Grey-scale representation of variability in HD 157246 (1993).

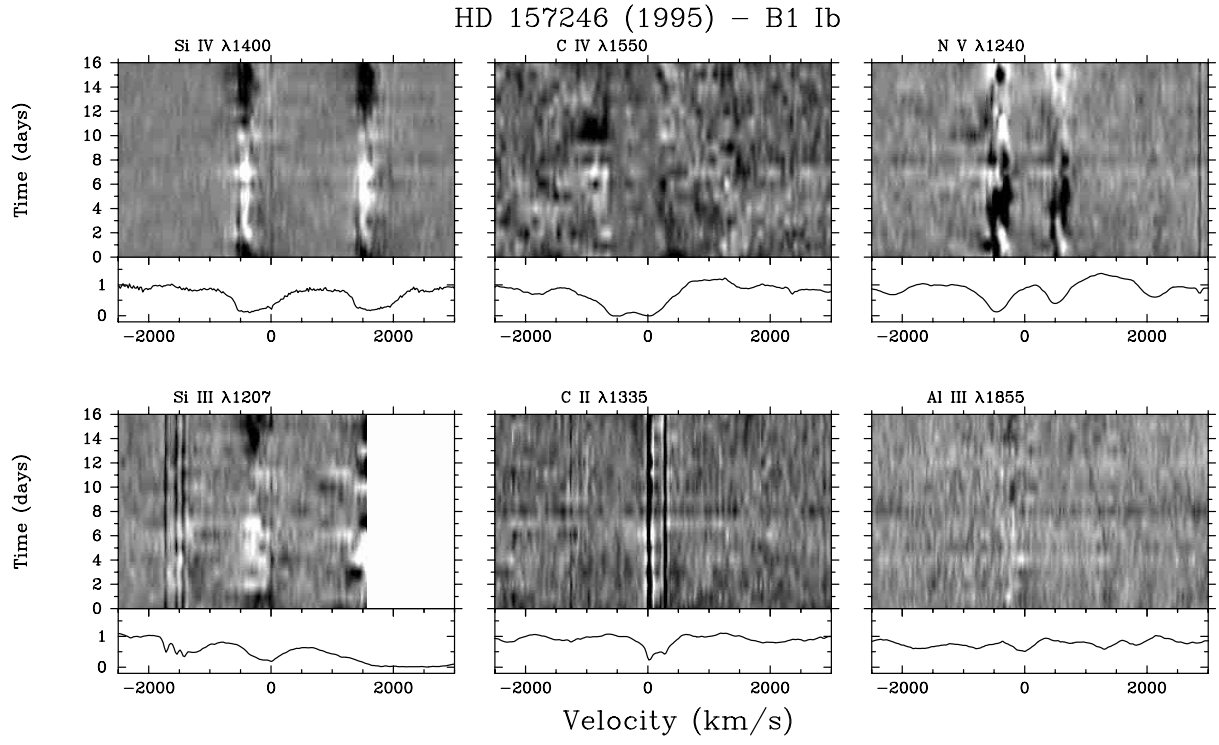

Fig. 15. Grey-scale representation of variability in HD 157246 (1995).

spectrum j measured in an adjacent continuum band, and $\sigma_0^2 = \left[\frac{1}{N}\sum_{j=1}^{N}\sigma_{cj}^{-2}\right]^{-1}$. The results are shown as root mean square percentages ($= TVS^{\frac{1}{2}} \times 100$) in Fig. 18. In all the stars with extended time-series data (i.e. spanning more than a few days), the absorption variability in Si IV is observed to extend down to less than 0.1 v_∞, and to essentially rest velocity in a few cases (e.g. HDs 64760, 150168, 47240 and 157246). This is a lower velocity than is generally the case for O-type stars, and the result suggests that

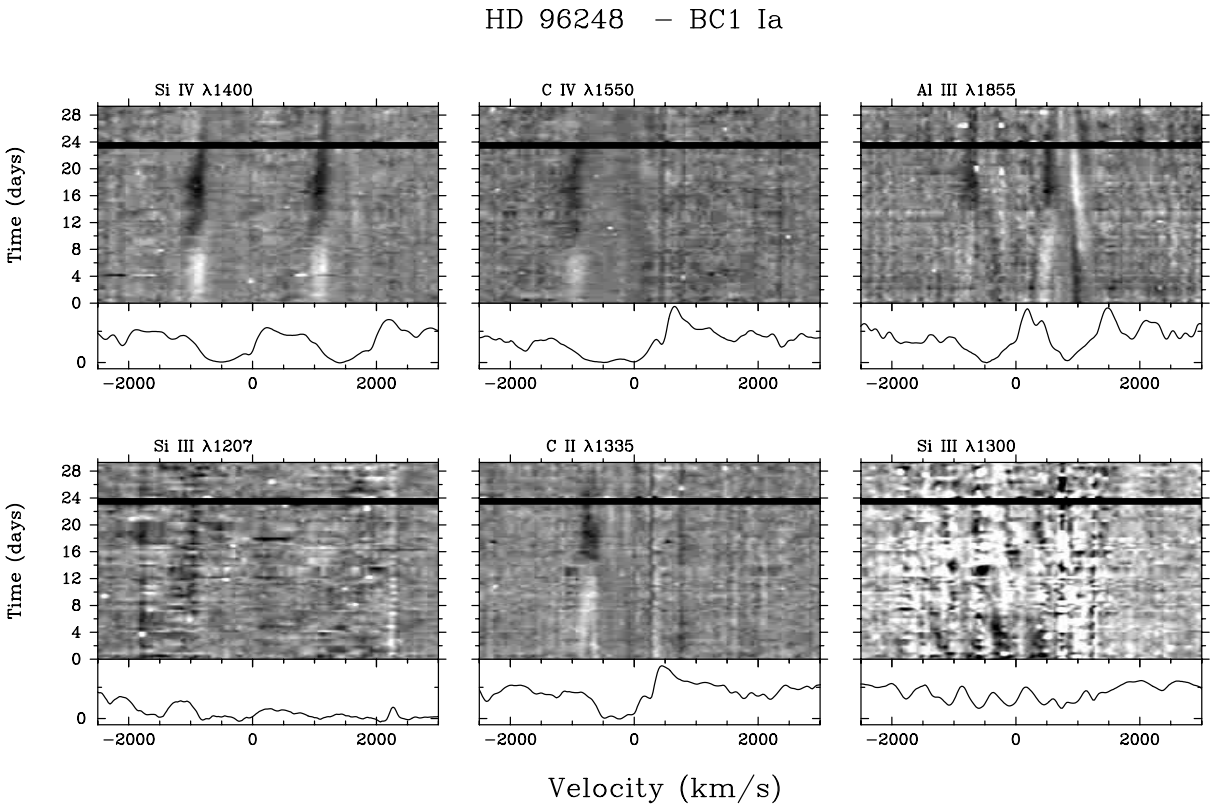

Fig. 16. Grey-scale representation of variability in HD 96248.

the winds of B stars are structured differently. Greater variability in the lower velocity portion of the P Cygni profiles in BIs indicates a lack of forward-scattered emission compared to O stars. This could be due to a multiply non-monotonic velocity law (which implies a higher degree of structure) or large-scale deviations from spherical symmetry (which decrease the net amount of forward scattering) or clumping (less scattering in all directions).

The maximum amplitude of the variations in Fig. 18 mostly occurs between ∼0.7 to 0.9 v_∞. HD 91969 and HD96248 exhibit the largest amplitude changes in Si IV. Though the variance diagnostics in Fig. 18 reveal no case of substantial variation in the emission components of the P Cygni profiles, weak systematic changes have been noted in the UV emission lobes of HD 64760 (e.g. Fullerton et al. 1997).

Measurements were also made of the ratios of minimum flux to maximum flux as a function of velocity for selected lines in the time-series data of each star. The overall trend in N V, Si IV and C IV is of a gradual decrease in $F_{\rm min}(v)/F_{\rm max}(v)$ (i.e. greater relative absorption or optical depth) with increasing velocity. The mean ratios (over all stars) vary as: $F_{\rm min}(v)/F_{\rm max}(v)$[N V] ∼ 0.81 (at 0.2 v_∞) to 0.68 (at 0.7 v_∞), $F_{\rm min}(v)/F_{\rm max}(v)$[Si IV] ∼ 0.80 (0.2 v_∞) to 0.33 (0.7 v_∞), and $F_{\rm min}(v)/F_{\rm max}(v)$[C IV] ∼ 0.53 (0.2 v_∞) to 0.05 (0.7 v_∞). The most extreme variations in lines other than Si IV (Fig. 18) occur in HD 150168 and HD 47240 in N V and C IV. The weaker Al III flux ratios do not exhibit a clear trend in velocity and mean values vary between ∼0.75 to 0.9 – stronger absorption variations are seen in this line in HDs 47240, 157246 and 96248.

4.1. Rotational modulation

Aside from the data sets of HD 91969 (Fig. 3) and HD 64760 (1995; Fig. 10), the remaining *IUE* time-series data of the program stars do not reveal unambiguous evidence for repeatable or cyclic modulations. In several cases this is likely because the *IUE* observations are not extended enough to cover stellar rotational time-scales. We nevertheless performed a Fourier period-finding analysis, using the CLEAN algorithm (Roberts et al. 1997) to iteratively remove the window function from the Fourier spectrum. We examined all the N V, Si IV and C IV time-series data sets for the program stars (where the line profiles had been previously normalised to the local continuum). The results indicate that (excluding HD 91969 and HD 64760) the only other cases of marginal significance where power is apparent across a reasonable fraction of the absorption trough (i.e. over few hundred km s^{-1}) are (i) a modulation of ∼4 days in the 1993 data set of HD 204172 (Fig. 8), and (ii) fluctuations on ∼1 day in the N V data set of HD 150168 (Fig. 12).

Variability in the Si IV lines is compared more directly in the images shown in Fig. 19, where the stars are ordered in terms of estimated maximum rotation period. There is perhaps some overall similarity between the moderate rotators HDs 47240, 204172, 164402 and 91969. Only

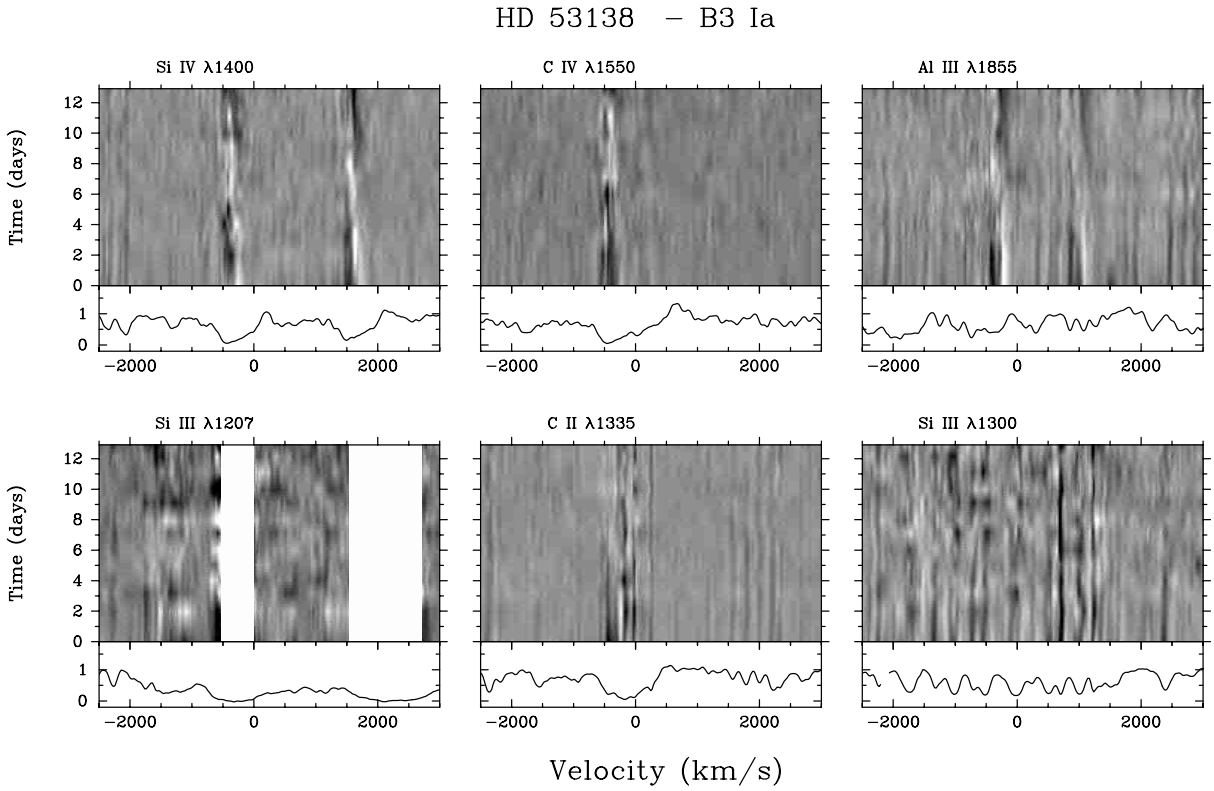

Fig. 17. Grey-scale representation of variability in HD 53138.

HD 150168 shows bowed features that resemble the striking patterns seen in HD 64760. There is also a resemblance between the very slowly propagating, high velocity DAC seen in HD 64760 (blue-wards of $\sim$−1200 km s^{-1}) and DACs seen towards the short-ward profile edge in HD 204172 and HD 164402.

In O-type stars the UV resonance line profile variability is usually dominated by the blue-ward migrating, recurrent, DACs. The apparent connection between modulated wind activity and stellar rotation in these stars is then based on measured trends in the recurrence and evolution time-scales of the DACs. We have shown in Sects. 3 and 4 that the line profile behaviour of BIs is more complex, such that the variance (e.g. Fig. 18) is generally not due to a single phenomenon such as DACs, but instead reflects the contributions of different variable structures. Furthermore, the empirical properties of these co-existing features do not all follow the same evolution time-scales. Examples of fairly localised (i.e. velocity widths $\sim$0.1 to 0.3 v_∞) blue-ward migrating features that resemble DACs in O-type stars are seen in our sample in HDs 91969, 164402, 64760 (1995), 150168, 157246 (1993) and 96248. The measured mean accelerations for the DACs in the highest $v_{\rm e}$ sin(i) stars, HDs 64760 and 157246, are $\sim$90 km s^{-1} d^{-1} and 140 km s^{-1} d^{-1}, respectively. The corresponding values for the slower rotators, HDs 96248, 150168 and 164402 are $\sim$ 7 km s^{-1} d^{-1}, 35 km s^{-1} d^{-1} and 20 km s^{-1} d^{-1}. Therefore, aside from the other variability phenomena identified in Sect. 3.1, these results are consistent with the view that the time-scale of stellar wind activity in radiation-pressure-driven, luminous early-type stars is related to the rotation period of the underlying star. However, our study also highlights other broad absorption features which can arise and evolve substantially over comparatively short time-scales ($\sim$1 to 2 days) in seemingly moderate or slow rotators, such as HD 204172 and HD 150168 (see e.g. Fig. 19).

5. Profile fitting with the SEI code

In this section we present the results from wind line profile modelling, to derive further details of the UV variability characteristics and ionization states of early B supergiants. Specifically, our objective was to derive values for the product of mass-loss rate and ion fraction ($\dot{M}\,q_i$), for the mean line profiles of the time-series and for cases of overall maximum and minimum observed absorption. We also examined trends in the relative ionization ratios. Our approach in this analysis is limited to the simplified method of employing steady-state line synthesis models to match observed profiles that are obviously affected by temporal wind structure and inhomogeneities in the outflow. Nevertheless, some useful information can still be derived from the success and failures in matching line profiles due to different ions.

We modelled the N V, C IV, Si IV and Si III (λ1207) wind lines (and in a few cases also Al III and C II) using the

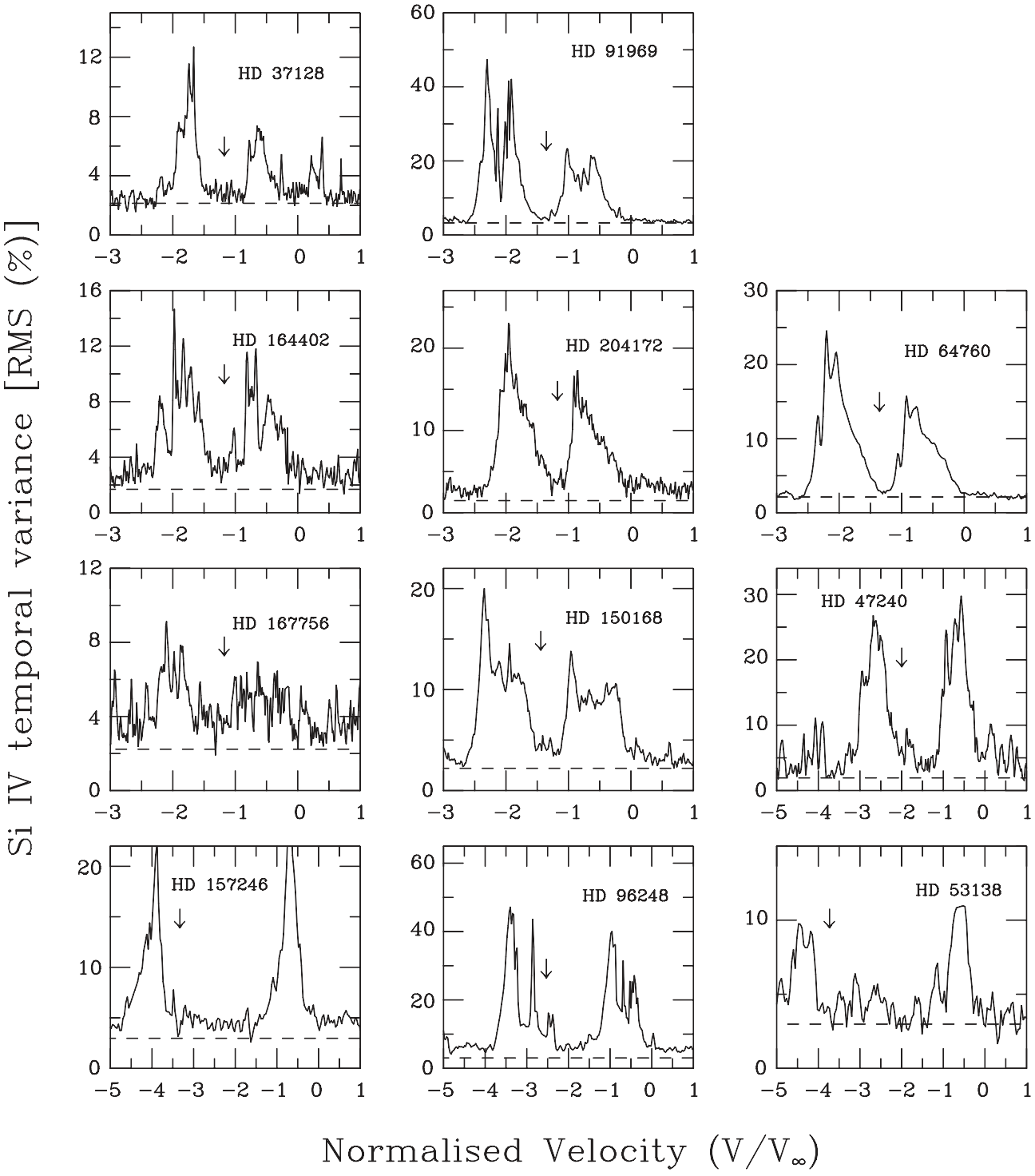

Fig. 18. Temporal variance (rms) for the Si IV spectral lines in our program stars. The velocity scale is with respect to the *red* component of the doublet, and the rest wavelength of the blue component is marked by an arrow. The horizontal dashed lines mark the level of significance for a probability of 95%.

"Sobolev with exact integration" (SEI) method described by Lamers et al. (1987). In addition, we adopted the modified treatment of the wind optical depth law introduced by Massa et al. (1995b), such that the radial optical depth $\tau_{\rm rad}(w)$ is treated in 10 independent velocity bins (each 0.1 v_∞ wide). This approach provides greater flexibility in matching absorption optical depths in a wind that is affected by time-variable structure. We assume a standard parameterised law for the wind of the form

$$w = w_0 + (1 - w_0)(1 - 1/x)^\beta, \quad (2)$$

where $w = v/v_\infty$ and $x = r/R$, where R is the stellar radius. We select $\beta = 1.0$ and $w_0 = 0.01$, and generally find that the model profiles do not differ grossly for values

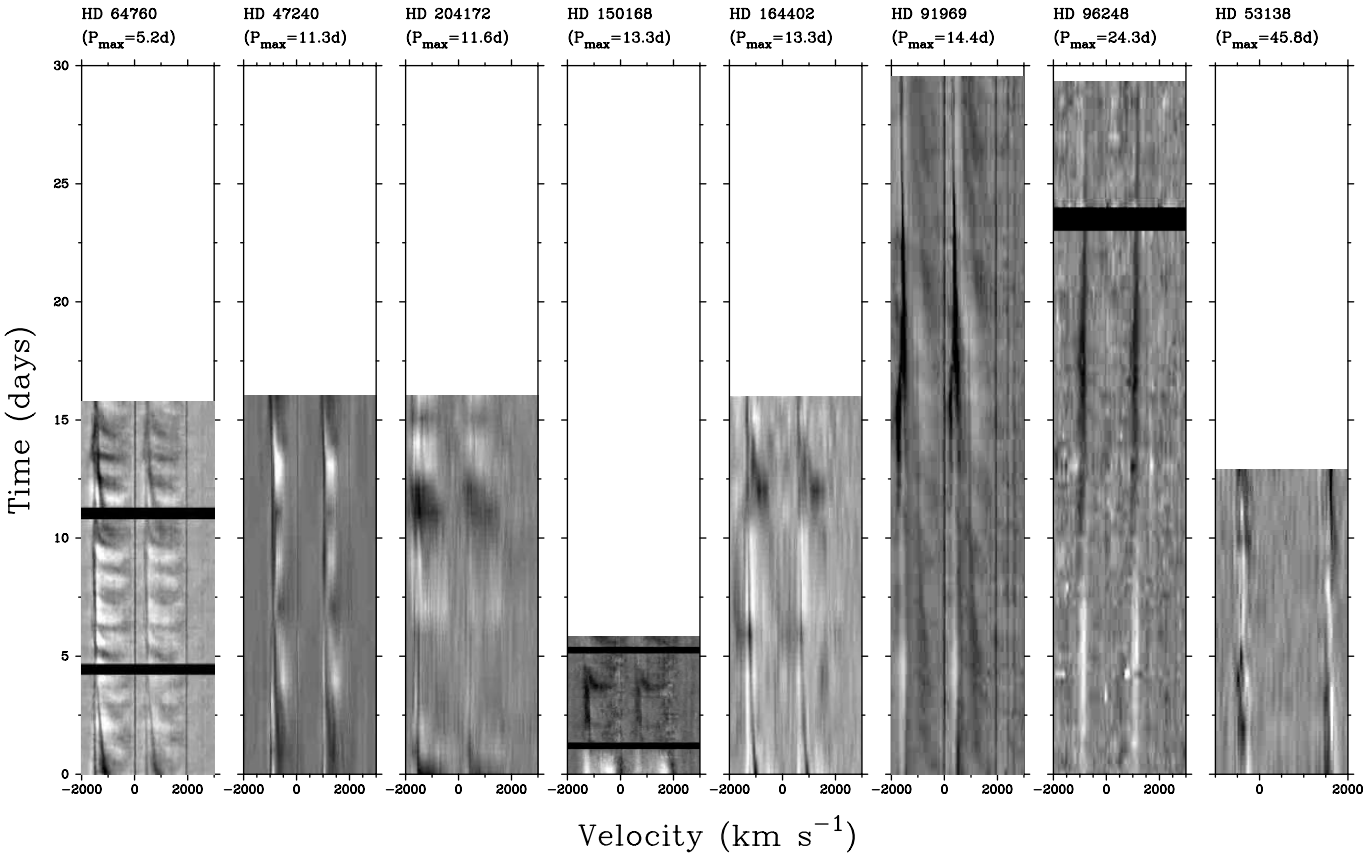

Fig. 19. Comparison of the Si IV variability characteristics of selected program stars; the estimated maximum rotation period is increasing from left to right.

of β between 0.5 to 2.0. A range of 0.05 to 0.1 was adopted for $v_{\rm turb}$, which is the small-scale velocity dispersion parameter (i.e. the localised velocity dispersion is typically $\sim$100 km s^{-1}).

Since the UV photospheric spectrum of early BIs can be fairly strong, it is necessary to allow for their effects in the SEI profile fitting. The high-resolution *IUE* photospheric spectra of the following stars were adopted (by spectral type) as "standards" and explicitly included as a lower boundary for the calculations: HD 36512 (B0 V), HD 36960 (B0.5 V), HD 31726 (B1 V), HD 36959 (B1.5 V), HD 35468 (B2 III), HD 207330 (B2.5 III) and HD 209008 (B3 III). These "standard" stars were selected as low $v_{\rm e}\sin(i)$ targets, covering the range of spectral types of our program stars, and exhibiting very weak or no evidence for winds in their resonance lines. The input photospheric spectra were convolved with a rotational profile to match the rotational broadening of the program stars, and generally the agreement between the corresponding photospheric absorption lines was very good.

With the parameters in the velocity law and photospheric input fixed, the $\tau_{\rm rad}(w)$ bins were the only free parameters in the line fitting scheme. The procedure adopted was to fit the individual profile, bin by bin, progressing from the blue-ward profile edge to less negative velocities (see Massa et al. 1995b). We modelled in this manner the mean N V, C IV, Si IV, and Si III profiles for the time-series data of each program star. In addition, to gauge the range in parameters due to profile variability, we also modelled for N V, Si IV, and C IV, the representative (overall) maximum and minimum absorption spectra (the IUE SWP images used in these cases are listed in Table 4). The Si III λ1207 lines are generally too weak and their photospheric absorption lines are less well matched by the standard stars, to determine variability characteristics by profile fitting. Therefore only the results of fits to the mean Si III line profiles are quoted in Table 4. The mass-loss rate results are summarised in Table 4, where the $\dot{M}\,q_i$ values are integrated over 0.2 to 0.9 v_∞. Examples of the fits to the mean profiles are shown in Fig. 20. We note the following key points from this analysis.

The overall quality of the line profile matches is good, which partly reflects the flexible optical depth "law" adopted. It is notable that mostly in C IV – and to a lesser extent in Si IV – the low velocity absorption (i.e. below about $0.25v_\infty$) is not well matched. The spherically symmetric models often predict excess forward-scattered emission in the low-velocity part of the P Cygni absorption trough. The discrepancy scales qualitatively with the strength of a given spectral line, such that it is generally worse for the maximum absorption cases than the minimum ones for a single star. Puls et al. (1993) discuss in detail the fact that reduced emission results when account is taken of back-scattering in several different resonance

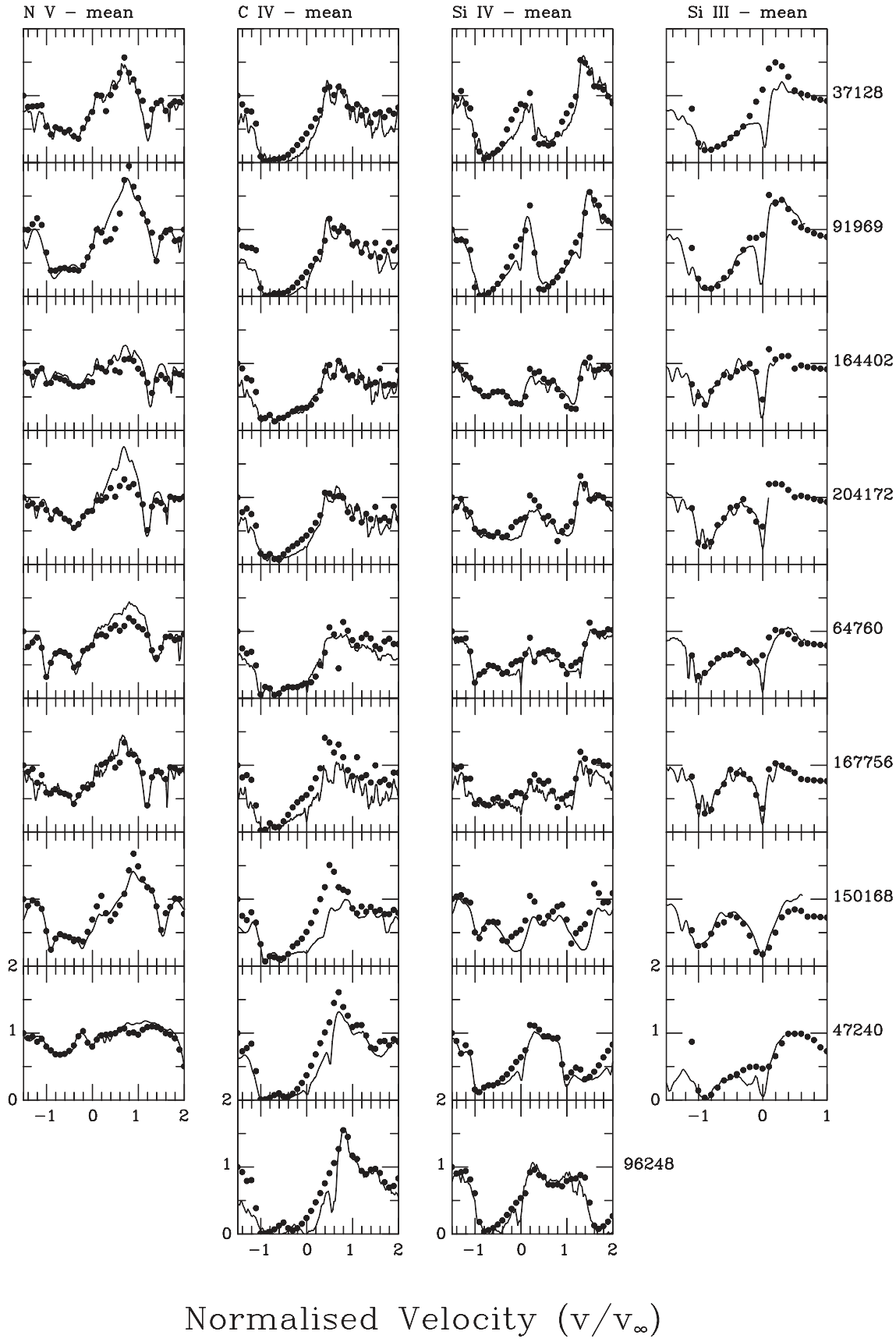

Fig. 20. SEI model line profile fits for N V, C IV, Si IV, and Si III lines in our program stars. Examples are shown for the cases of constructed mean profiles (see also Table 4).

Table 4. Results from SEI model profile fits.

		$\dot{M}\,q(\mathrm{N}^{4+})$		$\dot{M}\,q(\mathrm{Si}^{3+})$		$\dot{M}\,q(\mathrm{C}^{3+})$		$\dot{M}\,q(\mathrm{Si}^{2+})$
Star (HD)	v_∞	mean	range	mean	range	mean	range	mean
37128	1700	2.75(−9)	2.60–3.40(−9)	1.64(−8)	1.13–1.79(−8)	>4.79(−9)	–	1.56(−9)
91969	1500	4.31(−9)	4.00–5.25(−9)	1.60(−8)	0.88–1.60(−8)	>4.01(−9)	–	1.39(−9)
164402	1650	6.31(−10)	5.21–6.54(−10)	1.12(−9)	1.12–1.66(−9)	1.07(−9)	0.82–1.30(−9)	1.34(−10)
204172	1750	8.36(−10)	0.74–1.53(−9)	3.06(−9)	2.14–4.34(−9)	1.92(−9)	1.84–3.48(−9)	3.12(−10)
64760	1500	9.90(−10)	0.86–1.43(−9)	2.88(−9)	1.77–4.80(−9)	1.82(−9)	1.54–2.41(−9)	2.22(−10)
167756	1750	1.52(−9)	1.46–1.64(−9)	3.25(−9)	2.42–3.37(−9)	2.01(−9)	1.93–2.21(−9)	3.70(−10)
150168	1370	5.30(−9)	4.76–6.98(−9)	3.58(−9)	0.80–5.76(−9)	2.34(−9)	1.55–2.80(−9)	2.77(−10)
47240	1000	2.67(−10)	2.65–3.87(−10)	2.57(−9)	2.20–5.43(−9)	>1.28(−9)	–	6.49(−10)
157246	600	7.30(−10)	7.00–14.30(−10)	9.80(−10)	5.70–16.50(−10)	>4.61(−10)	–	–
96248	800	–	–	1.46(−9)	1.45–1.46(−9)	5.81(−9)	4.29–6.03(−9)	–
53138	520	–	–	2.78(−9)	2.55–3.07(−9)	7.27(−10)	7.20–7.97(−10)	–

The products of mass-loss rate and ionization fraction ($\dot{M}\,q_i$) are derived from fits to the mean profiles. (X.XX(-Y) = X.XX × 10^{-Y} $M_\odot$ yr^{-1}). The range in this value determined from cases of overall minimum and maximum absorption is also listed. The *IUE* SWP images corresponding to the cases of minimum and maximum absorption that were modelled are: HD 37128 (8100, 8130), HD 91969 (57187, 57426), HD 164402 (54200, 54225), HD 204172 (38957, 48914), HD 64760 (53522, 53709), HD 167756 (29001, 29049), HD 150168 (47098, 47198), HD 47240 (48953, 48930), HD 157246 (54172, 54103), HD 96248 (57069, 57204), HD 53138 (30153, 30264). We also obtained a few results from fits to Al III – HD 204172, 2.72(−9); HD 47240, 2.47(−9); HD 96248, 3.38(−8) and C II – HD 53138, 6.84(−10).

zones in structured winds. The reduced emission acts so as to yield an apparent increased absorption in the low velocity region between ∼0 and $0.3v_\infty$. Also if the winds are not spherically symmetric, then the models will produce too much scattered light at low velocities. It is also possible that to some degree the mis-match at low velocities reflects clumping in a highly structured wind so that parts of the stellar disk are being obscured by very different amounts of material than others.

The mean values of $\dot{M}\,q_i$ listed in Table 4 are consistent with the dependence on luminosity for B supergiants reported by Prinja & Massa (1997), who presented preliminary results for a wider, time-averaged survey. Typically the range in $\dot{M}\,q_i$ implied by the variability between minimum and maximum absorption line profiles is a factor of ∼1.5. A clear exception is the factor of ∼7 change noted in $\dot{M}\,q(\mathrm{Si}^{3+})$ for HD 150168; this star showed strong evidence for ionization variability in the time-series data (e.g. Fig. 12 and see below). This quantity describes the change in structures integrated over a velocity range from 0.2 to 0.9 v_∞, and is therefore intended to reflect variations in the global mass-loss rate. However, the *localised* variations (i.e., in a given velocity bin) can be several times larger. For example, at 0.7 v_∞ (cf. temporal variance in Fig. 18), the product of $\dot{M}\,q(Si^{3+})$ may vary between a factor of 4 to 15 for supergiants in the spectral range B0 to B0.5. These changes reflect the degree of structure in the wind.

Our sample of stars is too small to derive useful information on the temperature dependence of the relative ion ratios. However, at a given effective temperature the values of $q(\mathrm{Si}^{3+})/q(\mathrm{N}^{4+})$, or $q(\mathrm{Si}^{3+})/q(\mathrm{C}^{3+})$, can differ by up to a factor of 5. We find that there are no significant differences (or trends) in an individual star between the relative ion fraction derived from the mean profiles, minimum absorption profiles and maximum absorption profiles. Over the spectral range B0 to B1 (Ia and Ib) the mean ion ratios are $q(\mathrm{Si}^{3+})/q(\mathrm{N}^{4+}) \sim 2.5$, $q(\mathrm{Si}^{3+})/q(\mathrm{C}^{3+}) \sim 1.7$ and $q(\mathrm{Si}^{2+})/q(\mathrm{Si}^{3+}) \sim 0.1$. HD 150168 and HD 157246 (γ Ara) exhibit the most exceptional mean ion ratios of $q(\mathrm{N}^{4+})/q(\mathrm{Si}^{3+})$. In HD 150168 the ratio is almost 3 times larger than for other stars of similar parameters. The difference is linked to the ionization change (of unknown origin) that occurred during the run (see Sect. 3.2); the increase in the ion ratio points to a temporal ionization shift from a "normal state" to a 'high state'. The ratio of $q(\mathrm{N}^{4+})/q(\mathrm{Si}^{3+})$ in γ Ara is also several times larger than for other BIs. This result may reflect a nitrogen rich stellar surface due to rotational mixing (in a rapid rotator). As expected, the $q(\mathrm{C}^{3+})/q(\mathrm{Si}^{3+})$ ratio of the BC star HD 96428 is abnormal, and the mean ratio is between 4 to 8 times larger than the other stars in our sample.

The behaviour of the ionic ratios as a function of velocity is shown in Fig. 21 for our program stars (based on fits to the mean profiles of the time-series). The $q(\mathrm{Si}^{2+})/q(\mathrm{Si}^{3+})$ ratio does not depend on abundance and its observed trend indicates a decrease in ionization state of the wind as a function of velocity. The relative ion mixture of $\mathrm{q}(\mathrm{Si}^{3+})/q(\mathrm{N}^{4+})$ seems to be more stable between ∼0.4 to 0.8 v_∞ (or ∼2 to 5 stellar radii for the adopted empirical velocity law).

HD 37128 (ϵ Ori) is the only star in our sample with a measured radio flux, which may be used to provide a reliable estimate of the mass-loss rate. Blomme et al. (2002) have conducted a radio and sub-mm study of ϵ Ori, and they derive a value of $\dot{M} = 1.9 \times 10^{-6}\ M_\odot\,\mathrm{yr}^{-1}$. The (mean) results in Table 4 therefore give ion

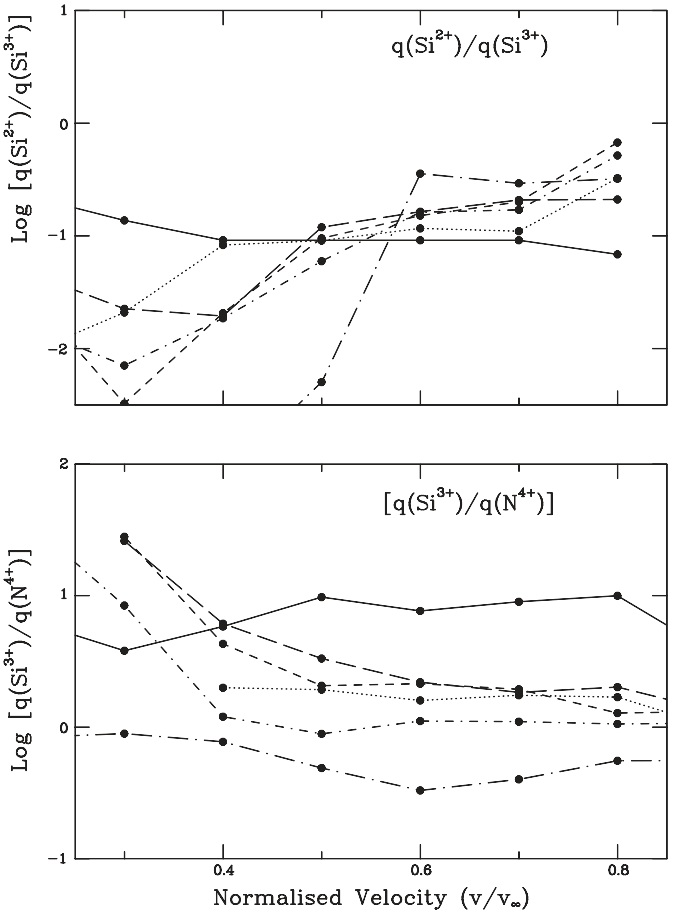

Fig. 21. The relative ion ratios (q_i/q_j) are plotted as a function of velocity, based on SEI model fits to the mean line profiles of our program stars.

fractions for this star of $q(\mathrm{N}^{4+}) \sim 1.5 \times 10^{-3}$, $q(\mathrm{Si}^{3+}) \sim 9.0 \times 10^{-3}$, $q(\mathrm{C}^{3+}) > 2.6 \times 10^{-3}$, and $q(\mathrm{Si}^{2+}) \sim 8.0 \times 10^{-4}$. Alternatively, using the theoretical mass-loss recipe of Vink et al. (2001) to determine the mass-loss rates for our target stars, yields mean ionization fractions over B0 to B1 of $\overline{q}(\mathrm{N}^{4+}) \sim 2 \times 10^{-3}$, $\overline{q}(\mathrm{Si}^{3+}) \sim 5 \times 10^{-3}$, $\overline{q}(\mathrm{C}^{3+}) \sim 3 \times 10^{-3}$, and $\overline{q}(\mathrm{Si}^{2+}) \sim 1 \times 10^{-3}$. The line-fitting analysis suggests therefore that none of the spectral lines modelled here represent the dominant stage of ionization for early B supergiants (over the UV line-formation region). This is particularly surprising for the case of Si^{3+} and C^{3+} in the earliest B stars studied, such as ϵ Ori. As in O-type stars, the other likely candidates for the dominant ion stages are Si^{4+}, C^{4+}, and N^{3+}.

It may be that the low ionization fractions derived here are due to the effects of clumping in the stellar winds (e.g. Massa et al. 2002, in preparation). If the winds are principally composed of optically thick clumps separated by transparent "voids", then each constant velocity surface will only partially contribute to the emission line. Furthermore, the face of the star would not be completely covered by optically thick material at any velocity. This means that the absorption part of the profile will not be very deep, thus also giving the impression of an unsaturated line. As a result, when fitting the spectral line with a homogeneous wind model, we derive a finite optical depth (and lower values of $\dot{M}\, q_i$), even though the optical depth of the wind might be much larger if the wind material was homogeneously distributed.

6. Discussion

We have shown that the stellar wind activity in early B supergiants is rich and varied. Figures 2 to 17 illustrate the fact that a selection of temporal signatures can occur in an individual star, and between stars. Different structures can also occur in the same star at different epochs, though γ Ara (HD 157246) is the only extreme example of this behaviour in our sample. The physical connection between these perturbations remains unresolved. There are two general forms of variability characteristics that appear to co-exist in the UV data *in some stars*:

1. Firstly there are broad absorption features which have a large spatial coherence (assuming monotonic velocity laws) and are relatively short-lived. Examples of these can be seen in HDs 64760 and 150168 as bowed features, and HDs 91969, 164402, 204172 and 47240 as blue-ward accelerating absorption enhancements.
2. In most of the stars listed above the broad absorption features are sometimes 'accompanied' by DACs, which are characteristically different in that they have longer temporal coherence. These features are much narrower in velocity, accelerate blue-wards more slowly, and are quickly confined to the highest velocities near the short-ward profile edge. Their origin is enigmatic partly because the UV time-series are mostly not extended enough to monitor the recurrence time-scales (and properties) of these features. It is therefore difficult to establish (or rule out) their connection to the extended absorption features (or bowed structures).

The first of the two phenomena are usually linked with the effects of CIRs (e.g. Owocki et al. 1995; Cranmer & Owocki 1996) passing through the line-of-sight. Specifically, localised features or inhomogeneities at the stellar surface are predicted to alter the radiative force, which leads to the formation of high-density low-speed gas streams. These streams are then rammed by the faster moving 'underlying' wind as the star rotates, leading to a spiral pattern. The enhanced absorption identified above arises from an extended layer of near-uniform velocity that marks the initial response of the unperturbed wind to the slower CIR ahead.

A further possibility then is that the slowly migrating DACs (item 2 above) are also related to CIRs, but originate in the radiative-acoustic kinks which are predicted to trail the CIRs in the hydrodynamical simulations of Cranmer & Owocki (1996).

It is important to realise that both observational phenomena highlighted above are not always present in every OB star. In many O-type stars for instance, only the long-lived DAC features are present, i.e. without evidence

for co-existing "bowed" structures or periodic absorption modulations. In this respect, we believe the "wavelength drift" model developed by Hamann et al. (2001) is more appropriate for a star with a distinctly structured wind such as HD 64760 (Fig. 10) or ξ Per (Kaper et al. 1997), than for ζ Pup where the dominant (19.2-hr) variability pattern is due solely to blue-ward migrating DACs.

The strong ionization changes seen in HDs 150168, 91969, 64760 and 157246 (Table 3) are likely shock signatures, though we cannot easily assign them to the same physical origin. If the interface between slow and fast wind streams in the CIR model is associated with strong shocks, then we can expect some ionization changes in the UV lines as the structure crosses the line-of-sight to the stellar disk. In cases where the variability phenomenon is seen at different velocities in different ions (Table 3), this behaviour may also relate to the action of spatially confined shock regions in the wind, where the post-shock gas is denser, lower speed, and less highly ionized than the pre-shock material. Mullan (1984) and Cranmer & Owocki (1996) discuss scenarios which may potentially result in velocity jumps of several hundred km s^{-1}.

An important result from our study is the variety of wind activity patterns that are present in the UV time-series data of BIs. However, this diversity of behaviour does not necessarily indicate that there is a corresponding variety of fundamental processes responsible for generating wind structure. The combination of stellar rotation rate and viewing (aspect) angle to the observer are among the most variable factors in our sample of B0 to B1 stars; more so than e.g. $T_{\rm eff}$, $\log(L_*)$, v_∞ and wind density. Inclination angle and $v_{\rm rot}$ could play an important role in determining the precise observational manifestation of azimuthally-extended large-scale wind structure that has its roots at the photosphere.

An interesting signature of spiral-shaped structure in a hot star wind is the appearance of bowed features. Since the winding of a spiral is determined by radial expansion and stellar rotation, the visibility of bowed features in UV time-series data is largely determined by the ratio of $v_{\rm rot}/v_\infty$. Though we only know the *projected* rotation velocity, and our statistical sample in this paper is small, the ratio of $v_{\rm e}\sin(i)/v_\infty$ is largest for HD 64740 ($\sim$0.14) and HD 157246 (γ Ara; 0.41 for 1995 data set). HD 64760 of course exhibits the clearest examples of phase bowing in our UV sample (Fig. 10), and indeed it is the best known case for this behaviour out of all the UV time-series data available for OB stars. Fast rotation is also undoubtedly the key to γ Ara's extreme behaviour, i.e. the *transient* two-component (polar and equatorial) wind. Interestingly, HD 150168 is the only other star in our study that shows bowed structures which are similar to those evident in HD 64760 (Fig. 12). The projected rotation velocity of this star is not exceptional and $v_{\rm e}\sin(i)/v_\infty$ is $\sim$0.09. This is possibly then an example where either the inclination angle and/or the density contrast of gas in the interacting spiral streams favours the detection of phase bowing.

We have discussed in this paper the best UV time-series data sets of early B supergiants available in any of the public archives. With the demise of *IUE*, these collections will not be improved for the forseeable future. One of our key objectives was to collect these homogeneous data sets into a single comparative study. Over the next few years these results will be complemented by extended time-series studies of luminous early-type stars in the Magellanic Clouds using the *Far Ultraviolet Spectroscopic Explorer* satellite (*FUSE*; $\lambda\lambda$900 to 1200). We anticipate in particular more sensitive searches for ionization variability in the far-UV lines, and an examination of the dependence of wind variability on metallicity. Additionally, $\sim$2 m class optical telescopes are currently being used to monitor time-dependent behaviour over rotational timescales in Balmer and He lines of OB supergiants. A key goal in these studies is to exploit the recombination-dominated lines to determine the coherence of large-scale wind structure in the deeper, near-star wind regions, close to potential photospheric inhomogeneities.

Acknowledgements. We are indebted to the staff at the NASA and ESA *IUE* Observatories at Goddard Space Flight Center, USA, and Villafranca, Spain for their hospitality and assistance. DM acknowledges support from NASA contract NAG5-7372 to Raytheon ITSS. This research made use of the Simbad database, which is operated at CDS, Strasbourg, France.

References

Bieging, J. N., Abbott, D. C., & Churchwell, E. 1989, ApJ, 340, 518
Blomme, R., Prinja, R. K., Runacres, M. C., & Colley, S. 2002, A&A, 382, 921
Cassinelli, J. P., Miller, N. A., Waldron, W. L., MacFarlane, J. J., & Cohen, D. H. 2001, ApJ, 554, L55
Cranmer, S. R., & Owocki, S. P. 1996, 462, 469
De Jong, J. A., Henrichs, H. F., Kaper, L., et al. 2001, A&A, 368, 601
Dufton, P. L. 1972, A&A, 16, 301
Ebbets, S. 1982, ApJS, 48, 399
Feinstein, A., & Marracu, H. G. 1980, PASP, 92, 266
Feldmeier, A. 1995, A&A, 299, 523
Feldmeier, A., Puls, J., & Pauldrach, A. W. A. 1997, A&A, 322, 878
Frost, E. B. 1909, ApJ, 29, 233
Fullerton, A. W., Gies, D. R., & Bolton, C. T. 1996, ApJ, 390, 650
Fullerton, A. W., Massa, D. L., Prinja, R. K., Owocki, S. P., & Cranmer, S. R. 1997, A&A, 327, 699
Garrison, R. F., Hiltner, W. A., & Schild, R. E. 1977, ApJS, 35, 111
Giddings, J. R., Rees, P .C. T., Mills, D., & Clayton, M. J. 1995, Starlink User Note 37, PPARC, Didcot
Gry, C., Lamers, H. J. G. L. M., & Vidal-Madjar, A. 1984, 137, 29
Hamann, W.-R., Brown, J. C., Feldmeier, A., & Oskinova, L. M. 2001, A&A, 378, 946
Henrichs, H. F., Kaper, L., & Zwarthoed, G. A. A. 1988, in A Decade of UV Astronomy with the IUE Satellite (ESA SP-281), 2, 145

Hiltner, W. A., Garrison, R. F., & Schild, R. E. 1969, ApJ, 157, 313
Howarth, I. D., Prinja, R. K., & Massa, D. L. 1995, ApJ, 452, L65
Howarth, I. D., Seibert, K. W., Hussain, A. J., & Prinja, R. K. 1997, MNRAS, 284, 265
Howarth, I. D., Townsend, R. H. D., Clayton, M. J., et al. 1998, MNRAS, 296, 949
Humphreys, R. M. 1978, ApJS, 38, 309
Humphreys, R. M., & McElroy, D. B. 1984, ApJ, 284, 565
Jarad, M. M., Hilditch, R. W., & Skillen, I. 1989, MNRAS, 238, 1085
Kaper, L. 1993, Ph.D. Thesis, University of Amsterdam
Kaper, L., Henrichs, H. F., Nichols, J. S., et al. 1996, A&AS, 116, 257
Kaper, L., Henrichs, H. F., Nichols, J. S., & Telting, J. H. 1999, A&A, 344, 231
Kaufer, A., Stahl, O., Wolf, B., et al. 1996, A&A, 305, 887
Kahn, S. M., Leuteregger, M. A., Cottan, J., et al. 2001, A&A, 365, L312
Lamers, H. J. G. L. M., Cerruti-Sola, M., & Perinotto, M. 1987, ApJ, 314, 726
Lennon, D. J., Dufton, P. L., & Fitzsimmons, A. 1992, A&AS, 94, 569
Levato, H., Morrell, N., Garcia, B., & Malaroda, S. 1988, ApJS, 68, 319
Lucy, L. B. 1983, ApJ, 274, 372
Lucy, L. B., & White, R. L. 1980, ApJ, 241, 300
Massa, D. 1989, A&A, 224, 131
Massa, D., Fullerton, A. W., Nichols, J. S., et al. 1995, ApJ, 452, L53
Massa, D., Prinja, R. K., & Fullerton, A. W. 1995b, ApJ, 452, 842
Massa, D., Fullerton, A. W., & Prinja, R. K. 1998, in Cyclical Variability in Stellar Winds, ed. L. Kaper & A. W. Fullerton (ESO Astroph. Symp., Springer, Berlin), 121
Morgan, W. W., Code, A. D., & Whitford, A. E. 1955, ApJS, 2, 41
Morrell, N., & Levato, H. 1991, ApJS, 75, 965
Mullan, D. J. 1984, ApJ, 283, 303
Owocki, S. P., Castor, J. I., & Rybicki, G. B. 1988, ApJ, 335, 914
Owocki, S. P., Cranmer, S. R., & Fullerton, A. W. 1995, ApJ, 453, L57
Prinja, R. K. 1988, MNRAS, 231, 21P
Prinja, R. K., Howarth, I. D., & Henrichs, H. F. 1987, ApJ, 317, 389
Prinja, R. K., Massa, D., & Fullerton, A. W. 1995, ApJ, 452, L61
Prinja, R. K., & Massa, D. L. 1997, in Boulder-Munich II: Properties of Hot, Luminous Stars, ed. I.D. Howarth, ASP Conf. Ser., 131, 218
Prinja, R. K., Massa, D., Howarth, I. D., & Fullerton, A. W. 1998, MNRAS, 301, 926
Prinja, R. K., & Howarth, I. D. 1988, MNRAS, 233, 123
Puls, J., Owocki, S. P., & Fullerton, A. W. 1993, A&A, 279, 457
Roberts, D. H., Lehár, J., & Dreher, J. W. 1997, AJ, 93, 968
Savage, B. D., & Massa, D. 1985, ApJ, 295, L9
Scuderi, S., Panagia, N., Stanghellini, C., Trigilio, C., & Umana, G. 1998, A&A, 332, 251
Vink, J. S., de Koter, A., & Lamers, H. J. G. L. M. 2001, A&A, 369, 574
Walborn, N. R. 1972, AJ, 77, 312
Walborn, N. R. 1976, ApJ, 205, 419